2005-04-21

Establising a high-frequency standard reference sequence stratigraphy, sea-level curve, and biostratigraphy for Morrowan strata of the Lower Absaroka I time slice based upon the Bird Spring Formation, Arrow Canyon, Nevada

Kristen Phelps Briggs
Brigham Young University - Provo

ESTABLISHIING A HIGH-FREQUENCY STANDARD REFERENCE SEQUENCE STRATIGRAPHY, SEA-LEVEL CURVE, AND BIOSTRATIGRAPHY FOR MORROWAN STRATA OF THE LOWER ABSAROKA I TIME SLICE BASED UPON THE BIRD SPRING FORMATION, ARROW CANYON, NEVADA

by

Kristen P. Briggs

A thesis submitted to the faculty of

Brigham Young University

in partial fulfillment of the requirements for the degree of

Master of Science

Department of Geology

Brigham Young University

August 2005

BRIGHAM YOUNG UNIVSERSITY

GRADUATE COMMITTEE APPROVAL

of a thesis submitted by

Kristen P. Briggs

This thesis has been read by each member of the following graduate committee and by majority vote has been found to be satisfactory.

_____	_____
Date	Scott M. Ritter, Committee Chair
_____	_____
Date	Thomas H. Morris, Committee Member
_____	_____
Date	Brooks B. Britt, Committee Member

BRIGHAM YOUNG UNIVERSITY

As chair of the candidate's graduate committee, I have read the thesis of Kristen P. Briggs in its final form and have found that (1) its format, citations, and bibliographical style are consistent and acceptable and fulfill university and department style requirements; (2) its illustrative materials including figures, tables, and charts are in place; and (3) the final manuscript is satisfactory to the graduate committee and is ready for submission to the university library.

_____ _____

Date

Scott M. Ritter
Chair, Graduate Committee

Accepted for the Department

_____

Jeffrey D. Keith
Department Chair

Accepted for the College

_____

Dana T. Griffen
Dean, College of Physical and Mathematical Sciences

ABSTRACT

ESTABLISHIING A HIGH-FREQUENCY STANDARD REFERENCE SEQUENCE STRATIGRAPHY, SEA-LEVEL CURVE, AND BIOSTRATIGRAPHY FOR MORROWAN STRATA OF THE LOWER ABSAROKA I TIME SLICE BASED UPON THE BIRD SPRING FORMATION, ARROW CANYON, NEVADA

Kristen P. Briggs

Department of Geology

Master of Science

For the same reasons which prompted its ratification in 1990 as the Global Stratotype Section and Point for the Mid-Carboniferous boundary, namely, section completeness, abundant fossils, and excellent exposure, the Morrowan Arrow Canyon Bird Spring strata is recommended as a candidate standard sequence stratigraphic reference for the Morrowan portion of the Lower Absaroka I supersequence. The stratigraphic architecture of Morrowan strata in Arrow Canyon was largely controlled by high-amplitude (100-m), high-frequency sea-level changes. Outcrop data and facies stacking patterns define 59 fifth-order fundamental cycles. These fundamental cycles stack into ten third-order sequences with an average duration of 320 ka. Changes in both cycle thickness and fundamental cycle type indicate that the second-order sea-level curve

of Golonka and Keissling for the Lower Absaroka Ia supersequence should be modified to reflect rising sea-level from the Mid-Carboniferous boundary with maximum flooding conditions ~120 to 135 meters above the Mid-Carboniferous boundary, followed by falling sea-level to ~6 meters below the Morrowan-Atokan boundary in Arrow Canyon. Additionally, cycle diagnostic conodonts and foraminifera permit correlation of selected third-order sequences to basins containing time-equivalent strata.

ACKNOWLEDGMENTS

This project was possible because of funding by generous donors, including the sponsors of and donors to the Warren Van Pelt Scholarship (2001-02), the Virgil and Audrey Peterson Scholarship (2002-03), the Brigham Young University (BYU) Geology Department, the BYU College of Physical and Mathematical Sciences, Dr. Scott Ritter, and Brigham Young University. I am grateful to professors and students whose support, counsel, and examples have influenced both my education and my personal life. For their field assistance, I am indebted to Aaron Leavitt, David Shoore, Rebecca Stewart, Teagan Tomlin, Paul Jenson, Paul Richardson, Greg Melton and wife, Michelle Hurst, Matt Rojas, Dan Martin, and Julia Kahmann. I thank my thesis committee for their willingness to serve and for their guidance and suggestions, most especially Dr. Scott Ritter whose direction has been priceless. I am grateful to the BYU Geology staff for their kindness and all they have done and continue to do for me and other students. I appreciate the employment and learning opportunities I had at BYU, Utah Valley State College, and Wagner Petrographic during my years as a graduate student. I thank my mom for instilling in me a love for learning, and my family for supporting their daughter and sister who “loves” rocks. Most importantly, I thank my friend and husband, whose confidence in me has taught and supported me through this educational journey.

TABLE OF CONTENTS

LIST OF TABLES

LIST OF FIGURES

INTRODUCTION

Recently, Golonka and Keissling (2002) subdivided the Phanerozoic Eonothem into 32 time slices (supersequences) bounded by second-order unconformities that can, in principle, be correlated globally and linked to global tectonic events and low-order eustatic sea-level changes. Ultimately, each of these time slices could be subdivided into third-, fourth-, and fifth-order events in order to construct a high-resolution sequence stratigraphic framework for the entire Phanerozoic Eon. During the past few years, the need for a more clearly defined Paleozoic sea-level curve has been expressed (Simmons, 2004). The sea-level curves constructed by Ross and Ross (1988) are being superseded by curves constructed for more specific time intervals based upon high-resolution stratigraphic studies of key stratigraphic sections (Simmons, 2004). This study develops a standard reference sequence stratigraphy and sea-level curve for the Morrowan portion of Golonka and Keissling's (2002) Lower Absaroka I time slice (Figure 1) based on the exceptional and continuous outcrops of Morrowan strata located in Arrow Canyon, Clark County, Nevada. In the process of developing this standard reference sequence stratigraphy and sea-level curve, three essential objectives were met by constructing (1) a standard facies association classification scheme, (2) a standard third- and fifth-order sequence stratigraphy, and (3) a sequence biostratigraphic framework for the Morrowan strata. Compiled data will be made available to other geologists via a specified website and interactive CD-ROM.

LOWER ABSAROKA I TIME SLICE

The Lower Absaroka I time slice, as defined by Golonka and Keissling (2002), is equivalent to the lower portion of Sloss' (1988) Absaroka sequence and ranges in age from 323-296 Ma. It consists of two supersequences, starting at the lower Bashkirian unconformity and continuing through to the upper Kasimovian unconformity (Golonka and Keissling, 2002). The lower of these (Bashkirian supersequence) is poorly represented globally except in the southwestern United States and in northeastern Europe where the supersequence was subdivided into seven and nine higher order transgressive-regressive depositional sequences, respectively by Ross and Ross (1987, 1988).

In this paper we formally name the Bashkirian depositional unit the Lower Absaroka 1a supersequence and provide a detailed higher order subdivision of this supersequence based upon microfacies stacking patterns, the evaluation of significant surfaces, and occurrences of biostratigraphically useful fossils in the Arrow Canyon section. In Arrow Canyon, this supersequence begins below the Mid-Carboniferous boundary in the Indian Spring Formation (exact location to be determined in future studies) and ends in lower Atokan strata at horizon A-240.

LOCATION, LITHOSTRATIGRAPHY, AND JUSTIFICATION

Arrow Canyon is located in Clark County, Nevada, approximately 80 kilometers northeast of Las Vegas, Nevada (Figure 2). The Bird Spring Formation, which was ratified as the Global Stratotype Section and Point (GSSP) for the Mid-Carboniferous boundary in 1990, was selected for this detailed study of the Lower Absaroka I supersequence because of section completeness, abundant fossils, and excellent

exposures. Decades of research from academia, industry, and government stratigraphers demonstrates that Arrow Canyon represents one of the most complete records of Carboniferous marine strata in North America (Rich, 1961; Lumsden, 1965; Cassity and Langenheim, 1966; Heath et al., 1967; Nowak, 1972; Pierce and Langenheim, 1974).

Morrowan strata, the focus of this thesis, comprise the lower 252 meters of the Bird Spring Formation as revised by Langenheim and Langenheim (1965) and Webster and Lane (1967). Continuous exposure of these beds permits complete facies sampling of carbonate cycles and reliable evaluation of facies stacking patterns, both of which are key to development of a standard reference sequence stratigraphy and sea-level curve.

In the 1960s, Amoco Oil Company geologists measured a stratigraphic section in Arrow Canyon from the top of the Mississippian Battleship Wash Formation through Virgilian-age (Gzhelian) strata of the upper Bird Spring Formation. Along this outcrop, they placed brass markers at 1.5-meter intervals, labeled consecutively from A-1 to A-579. Although many of these markers are now missing, they are the only reference points remaining in Arrow Canyon. Stratigraphic markers placed by other workers, such as Langenheim and Langenheim (1965) and Webster (1969), were removed in the late 1990s by the Bureau of Indian Affairs. For the sake of correlation to previously published reports on Arrow Canyon, the sequence stratigraphic framework outlined in this paper is linked to the Amoco reference markers. The Morrowan section begins at the Mid-Carboniferous boundary defined by the first occurrence of *Declinognathodus noduliferus* (located ~50 cm above horizon A-55) and continues up-section to the first occurrence of *Profusulinella spicata*, 20 cm below horizon A-224. Petrographic samples

were collected on both the south and north walls of the gorge as dictated by exposure and accessibility.

LATE CARBONIFEROUS PALEOGEOGRAPHY AND PALEOCLIMATOLOGY

During the Late Carboniferous, southern Pangea (Gondwana) straddled the South Pole, and northern Pangea, including present-day North America, was situated over the low latitudes (Francis, 1994). The Alleghenian orogeny continued along the eastern and southeastern portions of present-day North America and migrated westward to the Ouachita foldbelt (Golonka, 2002). Although subduction and mountain building existed along most of the western coast of Pangea, these tectonic events did not significantly effect deposition of the Bird Spring Formation. Arrow Canyon sat between 5-10°N latitude in the middle of a west-facing, distally steepened carbonate ramp on the southeastern portion of the Bird Spring-Ely trough as noted in Figure 3 (Stevens et al., 2001). This trough lacked a proximal siliciclastic source area, and fine-grained quartz found in this section was transported by northeast trade winds blowing across the western edge of the Ancestral Rockies (Stevens et al., 2001).

Glaciation in southern Pangea brought on global icehouse conditions, resulting in high-amplitude (50 to 100 m), high-frequency sea level changes driven by eccentricity (100- to 400-ka) and to a lesser degree by obliquity (40-ka) of the earth's orbit (Ross and Ross, 1985; Read, 1998; Soreghan and Giles, 1999). These sea-level fluctuations resulted in the deposition of the Late Carboniferous-Early Permian cyclothems in northern Pangea. Heath et al. (1967) and Nowak and Carozzi (1973) recorded over 90 such cycles in Arrow Canyon.

CLASSIFICATION METHODOLOGY

Methodology

The primary objectives in classifying Bird Spring facies were to (1) remain as true as possible to collected data and each rock's genetic origin, (2) create standard facies associations that would delineate significant aspects of each cycle, (3) use the compositional components of each sample to determine whether material was originally deposited, in what James (1997) termed, a heterozoan or a photozoan environment, and (4) create a standard facies classification methodology that is repeatable and can be used in other Carboniferous sections. When classifying carbonates based on petrographic data, critical features are texture and composition. Methodologies used to determine these features are described below and then related to environmental properties (i.e., energy level) in the facies associations that follow.

Outcrop data and fieldwork. Fieldwork in Arrow Canyon was conducted between March 2002 and November 2004. Candidate cycle boundaries, significant surfaces, and sedimentary structures were noted. Rock samples were collected at 20-cm to 2-m (0.72-m average) intervals through the entire Morrowan section. Standard petrographic thin sections were prepared for 345 samples.

Texture/rock fabric. Based on a modified version of Dunham's classification scheme, the textural classification of each thin section was determined visually and categorized as: mudstone, microbioclastic mudstone, wackestone, mud-dominated packstone, grain-dominated packstone, and grainstone (Appendix A).

Composition and statistical analysis. Geologists employ two methods in examining carbonate rocks, quantitative and semi-quantitative. The quantitative method

involves point-counting, while semi-quantitative analysis entails visually estimating the composition and texture of thin sections. In comparison with point-counting, some argue that semi-quantitative methods, as long as they are not inhomogeneous, produce comparable results, regardless of the kind of estimation (Flügel, 1982). Both methods have their pros and cons. Dennison and Shea (1966) noted that visual estimates are unbiased, but not precise. Although point-counting allows for more precision, it ignores size, shape, and sorting (Van der plas, 1965). Foraminifera and calcisphere abundances are better described by counting the total number of individuals in a thin-section area than by determining relative abundance from point-counting (Flügel, 1982). In recent years several authors have used multivariate statistics to determine facies groupings from point-count data (Khaiwka et al., 1981**;** Smosna et al., 1999**;** Westphal et al., 1999; Zempolich and Erba, 1999; Halfar et al., 2000). Herein, cluster analyses of point-count data were selected as the primary method of compositional analysis for 333 of 345 thin sections. Twelve samples could not be accurately point-counted based on composition because they were altered diagenetically. Once facies associations were determined, these samples were classified visually.

Three hundred points were counted for each thin section, utilizing 21 components: ooids/superficial ooids, oncoids/superficial oncoids, peloids, interparticle porosity, quartz grains, fusulinids, small foraminifera, coral, molluscs, microbioclasts, mud, bryozoans, brachiopods, crinoids, echinoids, phosphatic grains, trilobites, ostracodes, sponge spicules, algae, and intraclasts. Using SPSS® software, these data were used in two hierarchical cluster analyses, according to an agglomeration schedule/proximity matrix. Data standardization was not necessary because the same number of points (n=300) were

counted. Dendrograms were produced using between group (average) linkages over a squared Euclidean distance interval. All notes, point-count data, and compositional, textural, and facies classifications are stored in a database.

Heterozoan versus Photozoan Grain Associations

During the past three decades, warm- and cool-water carbonate environments have been the focus of study in the carbonate community (Lees and Buller, 1972). James (1997) further outlined the differences between warm- and cool-water carbonates and introduced the concepts of photozoan and heterozoan associations. The photozoan association includes shallow, warm-water, benthic calcareous communities and their resultant sediments, while the heterozoan association includes organisms and sediments that do not require warm, light-rich waters. Heterozoan components, unlike photozoan, are ubiquitous along a carbonate platform and have been so since they came into prominence during the Middle Ordovician. James added that photozoan elements are typically composed of reef-building taxa that have varied through time with the evolution and extinction of reefs. When photozoan sediments abound, carbonate deposition occurs along rimmed platforms and shelves. In contrast, heterozoan associations dominate carbonate ramps and open shelves (Burchette and Wright, 1992). Reef biota were not significant contributors to photozoan association sediments deposited along the Morrowan carbonate ramp of Arrow Canyon. Based on James (1997) and other publications (Lees and Buller, 1972; Beauchamp, 1994; Beauchamp and Baud, 2002), seven of the 21 compositional components studied herein are classified as photozoan components, including oncoids/superficial oncoids, peloids, ooids/superficial ooids, algae, molluscs, fusulinids, and intraclasts.

Based on visual analysis, the presence of any combination of these seven components, particularly of the non-skeletal grains, was significant enough that samples containing only 3% of these photozoan components showed characteristics of deposition in shallow-water, photic-zone environments (Figure 4). Thus, prior to clustering, the sample component data table was split into two smaller tables, using a 3% photozoan cutoff. The clusters formed from analysis of the greater than 3% photozoan data set were the foundation for the photozoan and transitional facies associations described below. Remaining samples (less than 3% photozoan components) were subjected to statistical analysis, and the resulting clusters formed the basis for the heterozoan, outer-ramp facies associations.

FACIES ASSOCIATIONS

Cluster analyses suggest the presence of three heterozoan, distal outer-ramp facies (Facies 0, 1, and 2); three heterozoan to transitional, proximal outer-ramp facies (Facies 3, 4, and 5); five photozoan, inner-ramp facies (Facies 6, 7, 8, 9, and 10); and one lowstand mixed siliciclastic-carbonate facies (Facies 11). These are described below (from most offshore to nearshore) and outlined in Table 1. Figure 5 contains representative photomicrographs and outcrop photos of each facies.

Heterozoan, Distal Outer Ramp

Distal outer-ramp (sub-storm wave base) conditions are represented by three mud-dominated facies designated, from deepest to shallowest, Facies 0, 1, and 2. Distinguished by the progression from laminated mudstone to burrowed mudstone to

burrowed wackestone, this facies suite reflects an up-ramp increase in oxygenation of the seafloor.

Laminated mudstone facies (Facies 0). This laminated mudstone facies consists of dark gray mudstone and silty mudstone interbedded with millimeter-thick laminae containing concentrations of quartz silt, calcareous microbioclasts (chiefly, finely comminuted crinoid and brachiopod debris), and/or sponge spicules. The grain-rich laminae form sites of localized silicification. Quartz silt grains, which comprise from 10 to 30% of this lithofacies, range from 10 to 50 microns in diameter and are typically subangular. Biological diversity is low, restricted to allochthonous microbioclasts. Burrowing is rare to absent. Where present, burrows (cf. *Zoophycus*) are mud-filled and noticeably flattened by compaction.

The preservation of laminae, predominance of fine-grained sediments, low biological diversity, limited infauna, and dark color suggest deposition in relatively deep, anaerobic waters, largely influenced by storm-suspended sediment. Grain-rich concentrations of eolian silt and allochthonous microbioclasts within the laminae represent distal gravity flows or distal tempestites. Distal laminated, outer-ramp sediments (2.9% of section) form the maximum flooding facies of four fifth-order cycles: B6.3, B7.3, B8.2, and B9.2.

Burrowed mudstone to sparse wackestone facies (Facies 1). Mud and silt-size microbioclasts are the dominant components of this fine-grained facies. Twenty to 30 micron-size subangular quartz silt (5 to 10%) may also be present. Rare larger skeletal grains include crinoid columnals and disarticulated to fragmented inarticulate and articulate brachiopods. Infrequent small foraminifera, calcispheres, sponge spicules,

trilobites, ostracodes, and phosphate grains may also be present. Sedimentary structures consist of rare burrows, which may be filled with spicule-rich packstone material. In the field, this facies displays medium to massive bedding. Lenticular to nodular chert is common.

The carbonate mud and microbioclastic debris that comprises the bulk of this facies (13.2% of section) was delivered to the outer ramp by sediment gravity flows and storm suspension, while quartz silt was transported by eolian processes. Destruction of laminae by an active infauna indicates a moderate increase in oxygenation of bottom sediments (dysaerobic conditions) over the laminated mudstone facies. This facies occurs as the maximum flooding facies of 11 fifth-order cycles: B4.2, B5.1, B5.3, B5.4, B6.1, B6.5, B7.2, B8.5, B9.3, B10.2, and B10.6.

Heterozoan skeletal wackestone facies (Facies 2). This facies, comprising 14.5% of the section, consists of medium- to thick-bedded skeletal wackestones to mud-dominated packstones. These rocks contain a typical Late Carboniferous heterozoan invertebrate fauna—crinoids (stem segments and disarticulated columnals), whole spiriferids and productids, complete to fragmented fenestrate and twiggy byrozoa, sponge spicules, sparse rugose corals, and rare trilobites. The matrix consists of dense micrite (partially altered to microspar and pseudospar) with variable percentages of microbioclastic debris. Distinct centimeter-scale burrows are evident in thin section. Compaction is indicated by “draping” of thin brachiopod shells over crinoid columnals and by the preferred horizontal orientation of grains. Chert nodules and lenses, both of which are common, contain concentrations of siliceous sponge spicules.

The abundant heterozoan marine fauna, intact skeletal grains, mud support, and pervasive burrowing indicate deposition on the outer ramp under well-oxygenated, low energy, subphotic conditions. Heterozoan skeletal wackestones document the maximum flooding facies of the following fifth-order cycles: B1.3, B1.4, B2.3, B2.6, B3.1, B3.3, B3.4, B3.5, B3.6, B3.7, B4.3, B7.1, B8.1, B10.3, B10.4, and B11.2.

Heterozoan to Transitional, Proximal Outer Ramp

The proximal outer ramp sat between fair weather and storm wave base and is represented by three heterozoan to transitional wackestone to packstone facies. Facies 3 was deposited during periods of rapid sea-level rise and is dominated by disarticulated brachiopod shells, subsequently over-packed. Facies 4, a crinoid-dominated packstone facies reflects intermittent development of offshore crinoid banks and sands. Two varieties of mixed heterozoan/photozoan wackestones to grain-dominated packstones facies dominate this portion of the ramp. Some samples contain 15 to 20% photozoan components and reflect increasing availability of light and/or storm transport of photozoan grains onto the proximal outer ramp, while those lacking photozoan components reflect deposition on the basinward side of the proximal outer ramp under storm-influenced, subphotic conditions. Because these two varieties were similar in texture and in their location within a cycle, they are grouped together as Facies 5 (see Figure 5I and J).

Transgressive skeletal packstone facies (Facies 3). Although not abundant (2.5% of section) volumetrically, this facies, which weathers to slopes, forms the basal transgressive unit of selected cycles (SO.2, B3.2, B3.7, B4.1, B5.1, B5.3, and B11.2). It is characterized by over-packed concentrations of whole to broken brachiopods and/or

disarticulated crinoid columnals. Other skeletal debris includes fragments of bryozoans, trilobites, conodonts, and inarticulate brachiopods. Irregular phosphatic grains and phosphatized skeletal grains are important components of this facies. Horizontal orientation of platy grains and frequent sutured grain boundaries indicate pervasive compaction. The matrix is comprised of dark gray to black organic-rich mud, some of which has been altered to microspar.

The concentration of skeletal grains, dark gray to black color, abundance of phosphatic grains, selective phosphatization, and compaction reflects slow sedimentation on the winnowed seafloor during rapid sea-level rise.

Over-packed crinoid packstone facies (Facies 4). This facies, accounting for only 0.9% of the Morrowan section, is characterized by abundant whole to abraded crinoid columnals (up to 64%) with subordinate amounts of brachiopod and bryozoan debris. Minor skeletal constituents include trilobites, ostracodes, molluscs, microbioclasts, and endothyrid, millerellid, and staffellid foraminifera. Over-packed packstone textures prevail in rocks of this facies, apparently as a result of mechanical and chemical compaction. Sutured and penetrative grain contacts are common, as is deformation of interstitial mud lumps and skeletal debris.

The massive to thick-bedded crinoidal packstone facies is interpreted to reflect prolific growth of crinoid meadows in moderately deep waters below fair weather wave base. Deposition in deep water is indicated by the lack of exposure features on top of crinoid packstone beds, their compositional similarity with fine-grained outer-ramp facies, and the lack of micritized borders on constituent grains. Additionally, grain over-packing suggests that the crinoid-rich sediments were not cemented prior to compaction,

as might be expected if the crinoid sands were deposited on a shallow, high-energy grain shoal subject to the influence of meteoric waters during relative sea-level fall.

Mixed heterozoan/photozoan wackestone to grain-dominated packstone facies (Facies 5). This facies consists of wackestone to dominantly packstone textures with medium- to coarse-sand size skeletal grains. The matrix is comprised of mud to fine-sand size fragments of crinoids and brachiopods. Abundant normal marine skeletal debris includes fragments of crinoids, articulate brachiopods, bryozoans, trilobites, inarticulate brachiopods, and echinoid spines. When present, photozoan grains comprise up to 15 to 20% of this facies while quartz silt (20 to 50 microns in diameter) abundances range from 0 to 15%. Photozoan carbonate material may include oncoids, peloids, gastropod and bivalve shells, calcareous sponge spicules, algae, and/or partially micritized grains. Many samples contain abundant endothyrid, biserial, staffellid, and millerellid foraminifers. In the field, this thick- to massively bedded facies weathers to form slopes and ledgy slopes. This facies comprises 33% of the Morrowan Series at Arrow Canyon.

Introduction of photozoan grains onto the proximal outer ramp was likely accomplished through an increase in ambient light on the landward portion of the proximal outer ramp and/or the downramp transport of photozoan grains from the adjacent inner ramp crest by storms and sediment gravity flows. In samples where only a diverse heterozoan fauna is present, the pervasive fragmentation of skeletal grains and packstone-dominated textures indicate deposition under well-oxygenated, intermittently storm-swept, subphotic conditions on the basinward portion of the proximal outer ramp.

The absence of graded tempestites and hummocky cross-stratification in this grain-rich facies is attributed to pervasive bioturbation.

Photozoan, Inner Ramp Facies

The inner ramp is located above fair weather wave base and is comprised of the high-energy ramp crest and low-energy lagoon facies belts. The former is characterized by photozoan-dominated grainstones and packstones (Facies 6, 7, 8, and 11), and the latter by mud-rich carbonates with a mixture of photozoan skeletal and non-skeletal components (Facies 9 and 10).

Oncoidal packstone to grainstone facies (Facies 6). This largely grain-rich facies comprises 7.1% of the entire section. Packstone textures prevail although oncoidal grainstones and wackestones occur. Oncoid abundances range from 12 to 75%. Other skeletal grains include whole to broken gastropods, bivalve fragments, trilobite fragments, crinoid columnals, foraminifera (coiled and irregular), calcareous algae, all of which may occur as oncoid nuclei. Micrite rims are common on skeletal grains. Non-skeletal contributors include ooids, superficial ooids, peloids, intraclasts, and small to moderate amounts of quartz (50-micron diameter). Below cycle B8.1, the cyanobacteria *Girvanella,* distinguished by its 10- to 50-micron diameter filaments, is the dominant oncoid-forming organism. Beginning in cycle B8.1, oncoid cortices are constructed by mixed *Osagia-Givanella* communities.

The abundance of oncoids indicates deposition in moderate- to high-energy environments along the inner ramp crest. Although present in many cycles, this facies forms the caprock to cycles B1.5, B2.2, B2.4, B7.4, B8.3, B8.5, B9.3, B10.2, B10.3, and B10.4.

High-energy shoal grainstone facies (Facies 7). This grainstone facies contains an abundance of finely comminuted, rounded, micritized skeletal grains in sparry calcite cement, and comprises 5% of the entire section. Compositionally, crinoid columnals dominate with lesser amounts of brachiopod and bryozoan debris. Minor molluscs, microbioclasts, coated grains, trilobites, ostracodes, algae, intraclasts, peloids, phosphatics, and small foraminifera may be present. In the upper portion of this section, near the Atokan boundary, fragmented coral and fusulinids are abundant. In addition to micritic rims, some grains may have superficial oncoidal or oolitic coatings. Sutured and penetrative grain contacts may be present. Cross-bedding is common on outcrop.

The presence of some algally coated grains, the abundance of abraded, micritized bioclasts, sparry calcite cement, and cross-bedding implies sedimentation in very shallow, high-energy shoal waters (less than 10 meters deep) that were exposed to meteoric waters during sea-level fall. This facies caps ten fifth-order cycles: SO.2, B1.3, B1.6, B2.5, B4.1, B4.4, B5.6, B8.1, B9.1, and B11.2.

High-energy laminated foreshore facies (Facies 8). The composition of samples in this facies varied with the availability of material from the adjacent ramp crest. Some samples contain peloid-rich layers interbedded with muddy or oncoid-dominated layers. In other samples, silt-size quartz grains and oncoids-rich layers are interbedded. However, all samples within this group have fine-scale planar to low-angle cross-bedded lamination indicative of a high-energy foreshore beach environment. This facies comprises 2.9% of the section and caps six fifth-order cycles: B1.2, B2.6, B5.5, B6.6, B7.2, and B9.4.

Lagoonal (peloidal) packstone to grainstone facies (Facies 9). Encompassing 6.9% of the section, this facies is dominated by thin- to massively bedded packstones containing peloids, fine-grained skeletal material, and/or quartz silt in a dark muddy matrix. Some microbioclasts and skeletal grains are superficially coated and gastropod and bivalve shells are common. Lesser amounts of small and irregular foraminifera, calcispheres, and intraclasts may be present.

The abundance of peloids, presence of molluscs, and dark muddy matrix of this facies indicate deposition in an organic-rich, protected lagoon on the landward side of the ramp crest. Lagoonal facies cap eight fifth-order cycles SO.1, B3.6, B3.7, B4.2, B4.3, B5.1, B6.4, and B8.4. Additionally, this facies is found in the shallowing upward portions of cycles B1.2, B2.1, B2.2, B2.6, B5.5, B5.6, B6.5, B8.3, and B9.3.

Peritidal laminite facies (Facies 10). This facies is extremely rare in the Morrowan Bird Spring Formation (0.5% of section). The rocks capping cycle B1.1 contain laminated, upward fining layers of silt-size microbioclasts and peloids. The succession of laminites just below the soil at the top of cycle B1.7 contain millimeter-thick, muddy laminae alternating with thin grainstone layers, rich in oncoids and fragmented skeletal grains. The laminated and cyclic nature of upward fining beds in this facies represent tidal flat deposition on the landward side of the ramp crest.

Lowstand mixed siliciclastic-carbonate facies (Facies 11). This facies (1.9% of section) is composed predominantly of fine-grained (50- to 200-micron diameter), moderately well-sorted, sub-rounded to subangular quartz grains. Some samples are cross-bedded and contain quartz-rich layers interbedded with bioclasts, which include rounded and micritized heterozoan skeletal grains, molluscs, algae grains and rare small

foraminifera. Quartz grains may be fused due to subsequent mechanical and chemical compaction. The abundance of quartz, cross-bedding, and location of these sands at the base of third-order sequences indicate these were eolian sands deposited during third-order exposure conditions and reworked in a high-energy shoal during ensuing lowstands. This facies is found in cycles B1.1 and B11.1.

Soil horizons. Soils consist of dark black mudstones to wackestones containing fenestral fabrics and cryptomicrobial laminae. Minor amounts of peloids, aggregates, skeletal grains, and authigenic quartz and feldspar may be present locally. Although extremely rare volumetrically (0.4%), soils form caprocks for three fifth-order cycles (B1.7, B7.1, and B10.6) and represent prolonged subaerial exposure.

DEPOSITIONAL MODEL FOR THE BIRD SPRING CARBONATE RAMP

Depositional facies indicate that Morrowan rocks at Arrow Canyon were deposited on a west-facing, carbonate ramp that lacked a proximal siliciclastic source area. Variable amounts of sub-rounded to subangular quartz silt and fine sand is attributed to eolian transport. Figure 6 illustrates the depositional profile and interpreted bathymetric range of each lithofacies. Sunlight, energy, and oxygenation of bottom waters increase from the distal outer ramp landward towards the grain-dominated ramp crest. Low-energy, inner-ramp lagoon and tidal flat laminites were deposited landward of the ramp-crest shoal.

High-order stratigraphic patterns were controlled by continuous moderate subsidence and high-amplitude, high-frequency icehouse sea-level fluctuation. During periods of transgression, slow sedimentation rates resulted in time-averaged accumulation

of heterozoan skeletal grains resulting in deposition of over-packed brachiopod and/or crinoid packstones (Facies 3). During maximum flooding, mud-rich heterozoan facies were deposited (Facies 0, 1, and 2). At times the seafloor was anoxic and laminations were preserved. During other highstands, oxygen permitted moderate to pervasive bioturbation of bottom sediments. Gradually, as accommodation space was filled and the seafloor sat between fair weather and storm wave base, crinoid-, brachiopod-, and to a lesser degree bryozoan-dominated heterozoan communities thrived, as reflected by Facies 4 and 5. As accommodation further decreased, both energy and light levels increased significantly along the ramp, resulting in deposition of grain-rich photozoan Facies 6, 7, and 11.

As relative sea level continued to fall, occasionally active foreshore beaches developed as material washed in from adjacent shoals (Facies 8). At other times, lagoonal back ramp conditions existed and energy levels dropped due to protection from various shoals and bar barriers. Micritized, rounded microbioclasts, peloids, mud, and molluscs (Facies 9) were deposited in these restricted settings. Although rare in this mid-ramp setting, tidal flat (Facies 10) and subaerial exposure conditions developed during times of maximum sea-level drawdown.

FACIES STACKING PATTERNS AND FUNDAMENTAL CYCLE TYPES

A significant part of facies interpretation is the stacking patterns of facies within a vertical facies succession. These vertical stacking patterns as well as outcrop data help delineate cycles. Recently, sedimentologists studying carbonate platforms (Sonnenfeld, 1996 and Giles, 1996) have moved away from establishing one ideal shallowing upward

cycle categorizing deposition along a platform in favor of a series of "fundamental" cycles that reflect the range of conditions that develop across a carbonate ramp during third-order sea-level cyclicity. Sonnenfeld (1996) defines fundamental cycles as the smallest resolvable vertical facies successions forming small-scale cycles. Sonnenfeld (1996) further notes that fundamental cycles are analogous to parasequences (Van Wagoner, 1985); however, facies successions within these fundamental cycles do not necessarily shallow-upward, particularly in solely subtidal cycles. In the Bird Spring section at Arrow Canyon, three types of fundamental fifth-order cycle types were noted. These cycles stack into third-order sequences and also reflect the transgressive and regressive stages of the Lower Absaroka Ia supersequence. The three fundamental cycle types are (1) *shallow photozoan cycles*, which frequently reflect shallow-water sedimentation that kept pace with accommodation, (2) *mixed photozoan/heterozoan cycles*, which are bounded by marine flooding surfaces, representing gradation from outer-ramp to inner-ramp conditions, and indicate that sedimentation caught up with accommodation, and (3) *deep subtidal cycles*, which indicate purely subtidal sedimentation that did not fill accommodation and often show evidence of non-Waltherian facies shifts. Examples of the fundamental cycles found in this section are illustrated in Figure 7. Each of the 59 cycles is categorized as one of the following fundamental cycle types and documented in Figures 8 and 9. Third-order sequences and fifth-order cycles are named based on their sequence stratigraphic position. For example, LAI-B1 means Lower Absaroka Ia supersequence, Bashkirian stage, third-order sequence 1; and LAI-B2.3 means Lower Absaroka Ia supersequence, Bashkirian stage, third-order

sequence 2, cycle 3 (note that S = Serpukhovian). For brevity, we have dropped the LAI-portion of cycle names in the text (i.e., LAI-B2.3 becomes B2.3).

Shallow photozoan cycles

Purely peritidal cycles were not found along this portion of the Bird Spring ramp; however, cycles containing predominantly photozoan facies, which may grade into foreshore packstones to grainstones, peritidal laminites or exposure surfaces, are present. Most of these cycles contain evidence of an active shoal environment and a few have a thin basal transgressive skeletal packstone which abruptly transitions to a shoal facies environment (i.e., SO.2 and B4.1). Shallow subtidal cycles are somewhat rare and seem to reflect third-order lowstand systems tracts imposed on the ramp. The following cycles serve as the base of third-order sequences and indicate lowstand systems tracts: B1.1, B1.2, B1.7, B4.1, and B11.1; other shallow photozoan cycles occur at the top of highstand systems tracts just below third-order sequence boundaries (cycles SO.1, SO.2, and B5.6).

Mixed heterozoan/photozoan cycles

These cycles typically begin with deep, outer-ramp facies overlying a marine flooding surface. The cycles are termed mixed heterozoan/photozoan because they grade upward from heterozoan, muddy outer-ramp facies into grainy photozoan-rich, inner-ramp facies, often rich in non-skeletal grains (i.e., oncoids and peloids; ooids are rare in Morrowan Bird Spring strata). Common caprocks are skeletal to oncoidal shoal and foreshore packstones to grainstones, with or without exposure crusts. In the upper portion of the Morrowan Series in Arrow Canyon (from cycle B6.6 upward), mixed

heterozoan/photozoan cycles rich in eolian siliciclastics are abundant, reflecting second-order sea-level fall during glacial phases.

Deep subtidal cycles

Deep subtidal cycles are composed of outer-ramp facies (Facies 0, 1, and 2) overlain by thinner, but grainy, proximal outer-ramp (Facies 5) to inner-ramp facies (usually Facies 9). These cycles reflect sedimentation that did not catch up with accommodation until sea level began to fall, frequently noted by the non-Waltherian facies shift from thick succession of subtidal outer-ramp facies overlain by relatively thin layers of shallow, inner-ramp facies (i.e., cycles B3.7, B4.2, B4.3, B4.4, B5.1). These cycles reflect second-order maximum transgressive and flooding conditions and also indicate third-order transgressive and highstand systems tracts.

CYCLE STACKING PATTERNS AND CYCLE HIERARCHY

Eustatic sea-level fluctuations occur due to global climate changes caused by perturbations in the earth's orbit around the sun, otherwise defined as Milankovitch cyclicity (Lehrmann and Goldhammer, 1999). Under icehouse conditions, high-amplitude, high-frequency (fourth- and fifth-order) sea-level fluctuations are superimposed on lower amplitude, low-frequency (third-order) sea level fluctuations (Lehrmann and Goldhammer, 1999). These third-order sequences, in turn, can stack into second-order supersequences. Second-order supersequences typically have durations ranging from 500 ka to 50 ka; third-order sequences last from 200 to 500 ka; fourth-order cycles occur between 100 to 200 ka; and finally, fifth-order cycles last from 10 to 100 ka. The Lower Absaroka Ia supersequence is a second-order supersequence with an

approximate duration of 27 Ma. The Morrowan Epoch lasted slightly less than 3.2 million years (Rice et al., 1994; Young and Laurie, 1995; Groves et al., 1999). Based on vertical facies stacking patterns, 59 fundamental cycles were identified in the Morrowan Bird Spring section. If we assume that near continuous sedimentation rates occurred along the carbonate ramp, we can calculate the average cycle periodicity by dividing the duration of the Morrowan by the number of Morrowan cycles in Arrow Canyon. This results in an average 54,000-year periodicity for each fundamental cycle; hence, these fundamental cycles reflect fifth-order sea-level changes. These 59 fifth-order cycles stacked into ten third-order sequences with an average time interval of 320 ka. Fundamental cycle stacking patterns reflected both second- and third-order sea-level fluctuations. The following section addresses how cycle architecture reflects second-order regressive and transgressive stages and how the stacking patterns of fifth-order fundamental cycles, the presence/absence of subaerial exposure surfaces, and a relative abundance curve outline third-order sequence boundaries and systems tracts.

Second-order Cyclicity

Figure 8 contains a second-order sea-level curve based on fundamental cycle stacking patterns. Unlike Golonka and Keissling's (2002) curve (Figure 1), the curve for the Lower Absaroka Ia supersequence (Figure 8) indicates that sea-level was already rising at the beginning of the Morrowan. Second-order lowstand conditions exist up through cycle B2.6. At the base of cycle B3.1, cycle morphology changes dramatically, reflecting the onset of second-order transgressive conditions. Cycles B3.1 through B3.5 comprise a series of thin (0.5- to 1-meter thick), deep subtidal cycles that contain a

relatively high abundance of transgressive skeletal packstones, suggesting deposition during rapid sea-level rise when accommodation remained unfilled.

This second-order sea-level curve denotes that sea level continued to rise during the formation of cycles B3.6 through cycle B6.1. Maximum flooding of the ramp occurred during the deposition of cycle B6.1, which records the longest period of sustained distal outer-ramp sedimentation. Cycle B6.1 is the thickest fundamental cycle at ~23 meters, which is five times the average (4.3 m) cycle thickness. Due to its anomalous thickness, we postulate that this cycle contains correlative conformities that could be correlated to shallower cycles upramp.

At approximately cycle B6.6, cycle morphology changes again reflecting a turnaround on the second-order sea-level curve from rising to falling sea. Cycles B6.6 through B8.2, largely designated as mixed heterozoan/photozoan cycles, form a series of 3-8 meter-thick cycles often capped by high-energy foreshore facies and subaerial exposure surfaces indicative of high-frequency cycles. Noticeable sea-level fall occurred during the deposition of these cycles and continued to fall through the deposition of cycle B10.6 as evidenced by shoaling-upward, mixed heterozoan/photozoan cycles and the increase in eolian siliciclastics.

Additionally, note the graphs to the left of the second-order sea-level curve on Figure 8. Based on point-count data, these graphs reflect the number of each component (i.e., quartz grains, oncoids, algae) per 300 in each thin section. Decrease in the abundance of quartz grains and oncoids coincides with maximum second-order flooding of the Bird Spring ramp.

Third-order Sequence Boundaries and Systems Tracts

Facies and cycle stacking patterns and the presence/absence of subaerial exposures surfaces define ten complete third-order sequences (Sequences LAI-B1 to LAI-B10) and their accompanying systems tracts. Sequence architecture is described below and graphically displayed on the detailed sequence stratigraphic chart (Figure 8) and the stratigraphic column (Figure 9). A relative abundance curve of heterozoan versus photozoan facies per fifth-order fundamental cycle was created as a proxy for sea-level changes (Figure 10). Ideally, turnaround points near 100% photozoan facies (0% heterozoan) should indicate the shallowest sea levels and, thus, correspond with sequence boundaries. Whereas, turnaround points with high heterozoan facies percentages should represent the deepest water conditions and correlate with maximum flooding surfaces. In some cases the significant surfaces determined by stacking patterns and outcrop data correlate well with turnaround points on the relative abundance curve (i.e., sequence boundaries for Sequence LAI-B2 and Sequence LAI-B4). For others, however, there is little correlation between the two (i.e., sequence boundary for Sequence LAI-B9). The location of significant surfaces, the range of third-order systems tracts, and cycle diagnostic conodont and foraminifer data (Amoco Production Company, unpublished) are described for each sequence.

Sequence LA1-S0 (incomplete). Only the upper 2.5 meters of this sequence (strata between the Mid-Carboniferous boundary and base of sequence LAI-B1) were studied as part of this project. This thin interval containing the upper part of cycle S0.1 and cycle S0.2 is biostratigraphically distinctive. *Declinognathodus noduliferus, Rhachistognathus primus, Rh. prolixus, Rh. websteri, Rhipidomella nevadaensis,* and *Turrispuroides*

multivoluta first occur at the Mid-Carboniferous boundary located at the base of cycle S0.1. This cycle also contains the last occurrence of *Brenckleina rugosa* and *Eosigmoilina robertsoni*. Cycle LAI-SO.2 boasts the first occurrences of *Globivalvulina bulloides* and primitive millerellids.

Sequence LAI-B1. This ~20.5-meter thick sequence is comprised of six cycles (B1.1 through B1.7). Although an obvious basinward shift in facies does not occur at the base of this sequence, the presence of reworked eolian sands at the base of cycle B1.1 indicates a long period of subaerial exposure indicative of third-order sequence boundaries. The lowstand systems tract consists of the lower portion of cycle B1.1 and contains ~1.5 meters of cross-bedded, very fine-grained quartz sandstone (Facies 11) at its base. The transgressive surface lies above these cross-bedded sands (just above horizon A-58). The transgressive systems tract is noted in this case by the gradual landward-stepping of cycles B1.2 through B1.3, which is a deep subtidal cycle. The maximum flooding surface (mfs) is located at the base of deep subtidal cycle B1.4, initiating the highstand systems tract which continues to the top of cycle B1.7. The top of this cycle contains a series of peritidal laminites (Facies 10) capped by a soil, indicating prolonged subaerial exposure characteristic of third-order sequence boundaries.

This sequence contains several distinctive faunal events that should permit its recognition both regionally and globally. Foraminiferal species that first appear in this stratigraphic unit include *Earlandia elegans* (BI.1), *Millerella marblensis* (B1.2), *Planoendothyra planiformis* (B1.2), *Endothyra bowmani* (B1.2), *Asteroarchaeodiscus bashkirikus* (B1.3), and *Planoendothyra aljutovika* (B1.5). Primitive eostaffellids first appears in cycle B1.2. *Gnathodus girtyi simplex*, which ranges upward from the Lower

Carboniferous, last occurs in limestones of cycle B1.1. Otherwise, conodont faunas from cycles B1.1 through B1.3 are essentially identical to those recovered from the underlying sequence. However, the upper meter of B1.3 contains the first occurrence of the early Late Carboniferous genus *Idiognathoides* (*I. sinuatus*). This is joined 30 cm higher in the base of Cycle B.4 by *Idiognathoides convexus,Rhachistognathus minutus minutus, Rh.. minutus havlenai* and *Neognathodus symmetricus*. The upper cycles of this sequence, B1.4 through B1.7 are characterized by a diverse assemblage of conodonts that include *Declinognathodus noduliferus, Rhachistognathus muricatus, Rh. primus, Rh. prolixus, Rh. websteri, Rh. minutus minutus, Rh. minutus, Rh. havlenai, Idiognathoides sinuatus, Idiognathoides convexus, Neognathodus symmetricus,* and *Adetognathus lautus*.

Sequence LAI-B2. Sequence LAI-B2 is ~19 meters thick, begins just above the soil horizon capping Sequence LAI-B1, and includes six cycles (B2.1 through B2.6). This sequence boundary corresponds with a turnaround point on the relative abundance curve (Figure 10). Cycle B2.1 is unique in that deposition occurred in gradually deepening waters, but nevertheless shallow, photic waters suggesting a very thin lowstand systems tract (lower three meters of cycle B2.1). The transgressive surface is just below horizon A-73, where shoal water grainstones (Facies 7) are overlain by subtidal mud-dominated packstones (Facies 5). The transgressive systems tract continues through cycle B2.2 to the base of deep subtidal cycle B2.3, which represents the sequence's mfs. Cycles B2.3 through B2.6 form the highstand systems tract and show evidence of gradual aggradation and progradation indicative of stillstand and falling sea conditions. The top of this sequence occurs at the base of cycle LAI-B3.1, where

proximal outer-ramp packstones are juxtaposed atop 1.5 meters of laminated foreshore grainstones (Facies 8).

This sequence contains most of the typical early Late Carboniferous conodont and foraminiferal species found in the underlying sequence. Subtle differences include the absence of *Rhachistognathus primus* and *Neognathodus symmetricus*, both of which disappear at the top of cycle B2.1. *Rhachistognathus websteri* last occurs approximately 2 meters higher in the top of cycle B2.2. *Idiognathoides sinuatus* last occurs in the middle cycle B2.4

Sequence LAI-B3. The transgressive surface and sequence boundary for Sequence LAI-B3 coincide at the base of cycle B3.1, leaving no record of a lowstand systems tract. The lower five cycles (B3.1 to B3.5) comprise the third-order transgressive systems tract and are comprised of transgressive lag deposits (Facies 3) interbedded with outer-ramp facies, indicating that the carbonate factory could not keep up with second-order sea-level rise. Maximum flooding facies are found at the base of cycle B3.6 in both thin section and outcrop data, indicating the commencement of highstand conditions which continued through to the top of cycle B3.7. This ~24.5-meter thick sequence is capped by 1.5 meters of lagoonal rocks (Facies 9).

With respect to conodonts, cycles B3.1 through B3.6 are indistinguishable from the underlying sequence. *Rhachistognathus muricatus,* however, last occurs in the caprock of cycle B3.1. Cycle B3.7 contains many holdover species including *Adetognathus lautus, Declinognathodus noduliferus, Rhachistognathus prolixus, Rh. minutus minutus, Rh. minutus havlenai*, and *Idiognathoides convexus*. It is distinguished from other cycles in the sequence by the first occurrence of two important Late

Carboniferous genera: *Idiognathodus* and *Streptognathodus*. *Neognathodus bassleri* also appears at this cycle.

Sequence LAI-B4. Cycle B4.1 is a shallow photozoan cycle that is out of place between the thick successions of deep subtidal cycles above and below it. One can infer that this cycle correlates with subaerial exposure and lowstand conditions further upramp. Thus, the base of cycle B4.1 serves as the basal sequence boundary for Sequence LAI-B4, which is ~16 meters thick. This sequence boundary coincides with a turnaround point on the relative abundance curve (Figure 10). Ramp conditions deepened rather abruptly at the top of cycle B4.1, denoting the base of the transgressive systems tract which consists of the lower portion of cycle B4.2 up through horizon A-103 where the mfs occurs. The highstand systems track continues up section to the top of cycle B4.4, where a thin layer of high-energy shoal grainstones (Facies 7) are overlain by transgressive packstones.

The lower cycle of this sequence contains the first occurrence of two new species of *Streptognathdus* (*S. suberectus* and *S. anteecentrucus*) and the last occurrence of long-ranging *Rhachistognathus prolixus*. Otherwise, the conodont fauna is comprised of holdover species from lower sequences.

Sequence LAI-B5. This sequence consists of ~33 meters that encompass cycles B5.1 through B5.6. The transgressive surface is coincident with the sequence boundary at the top of cycle B4.4. Because second-order transgressive conditions are well underway as indicated by the abundance of deep subtidal cycles, accommodation space is rarely filled in this sequence and determining the mfs is difficult. Over a meter and a half succession of heterozoan skeletal wackestones at the base of cycle B5.4 is the thickest

succession of distal outer-ramp facies within this sequence and was chosen as the mfs. Furthermore, cycles B5.5 and B5.6 shoal upward and prograde on top of cycle B5.4. Thus, the highstand systems tract is comprised of cycles B5.4 through B5.6. The top of cycle B5.6 contains a meter-succession of high-energy shoal grainstones capped by an erosion surface, indicating the third-order sequence boundary which initiates the next sequence. This sequence boundary roughly corresponds with a turnaround point on the relative abundance curve (Figure 10).

The key faunal events in this sequence are the first occurrence of pseudostaffellid foraminifera (base of cycle B5.1) and the disappearance of *Rhachistognathus minutus havlenai* (cycle B5.1), *Rh. minutus minutus* (cycle B5.2), and *Streptognathodus expansus* (cycle B5.6).

Sequence LAI-B6. This sequence, comprised of cycles B6.1 through B6.6), is the thickest (36.3 m) found in the Morrowan Bird Spring strata. Deep subtidal cycles dominate and second-order maximum flooding occurred during the deposition of cycle B6.1. The basal sequence boundary and transgressive surface are concurrent, and the transgressive systems tract continues up section for about three meters to the mfs just below horizon A-135. The highstand systems tract begins here and continues through cycle B6.6. Cycles B6.2 to B6.6 gradually thin, shoal upward, and prograde on top of each other, indicating third-order sea-level fall during the late highstand. Cycle B6.6 is a shallow photozoan cycle consisting of high-energy foreshore grainstones (Facies 8) capped by blackened exposure crusts containing rhizoliths. This exposure surface generally coincides with a turnaround on the relative abundance curve (Figure 10).

The base of this sequence is distinguished by the appearance of *Rhachistognathus minutus declinatus* and disappearance of *Streptognathodus suberectus* and *Idiognathoides convexus* approximately 3 meters above the base of cycle B6.1. *Streptognathodus angustus* appears in the upper part of this exceptionally thick cycle.

Sequence LAI-B7. The dominant fundamental cycle type shifts at the top of Sequence LAI-B6 from deep subtidal to a series of mixed heterozoan/photozoan cycles, meaning that fifth-order cycle sedimentation initially lagged behind the creation of accommodation but was able to catch up with sea level and fill accommodation by the cycle's end. As previously noted, second-order sea-level rise slows during this sequence, which is ~17-meters thick. It appears that on a high-frequency scale, sea level fluctuated greatly during this time along the ramp, dropping long enough for exposure features to form, yet rising high enough for distal outer-ramp facies to be juxtaposed atop cycle-capping exposures in cycles B6.6, B7.1, and B7.4.

The lowstand systems tract begins at the base of cycle B7.1 and consists of cycle B7.1 which is capped by a soil horizon. The transgressive surface occurs at the top of this cycle, where deep-water burrowed mudstones (Facies 1) overlie the soil. The transgressive systems tract is comprised solely of Cycle B7.2 and ends at the base of cycle B7.3, where a thick succession of laminated deep-water mudstones (Facies 0) represents maximum flooding. Highstand conditions continue from cycle B7.3 through B7.4, where this sequence is capped by an exposure crust overlying a meter-thick succession of oncoidal shoal facies (Facies 6).

Sequence LAI-B8. This third-order sequence consists of cycles B8.1 through B8.5 and is ~27 meters thick. Lowstand conditions are indicated by the presence of quartz silt

and cross-bedded high-energy shoal grainstones (similar to those found at the base of Sequence LAI-B4) of shallow photozoan cycle B8.1. Proximal outer-ramp facies overlying inner-ramp shoal facies at the top of cycle B8.1 represents the transgressive surface. The transgressive systems tract is thin, and maximum flooding occurs in a thick succession of laminated mudstones (Facies 0) a meter above the base of cycle B8.2 (about 50 cm above horizon A-178). Cycles B8.2 to B8.5 indicate gradual progradation as sea level fell during late highstand conditions. The top of cycle B8.5 represents the upper sequence boundary.

Sequence LAI-B9. The stacking patterns of this sequence parallel those of Sequence LAI-B8. Cycles B9.1 through B9.4 combine to form this ~19-meter thick sequence. As before, fundamental cycle stacking patterns indicate that lowstand conditions were imposed on the ramp, shown by the presence of the shallow subtidal cycle B9.1 overlain by a deep subtidal cycle. Cycle B9.1 is composed of mixed heterozoan/photozoan packstones capped by high-energy shoal grainstones which most likely correlate with tidal flat to exposure conditions further upramp. Sea level deepened suddenly atop this cycle representing a transgressive surface. The lower 1.5 meters of cycle B8.2 comprise the transgressive systems tract. Maximum flooding occurs in a 5.5-meter thick succession of distal-outer ramp facies between horizons A-196 to A-197, beginning the highstand systems tract which continues to the top of cycle B9.4. Cycles B9.3 and B9.4 shoal upward and prograde atop cycle B9.2. The capping sequence boundary at the top of cycle B9.4 is indicated by a basinward shift in facies where outer-ramp deposits (base of cycle B10.1) overly a 2-meter series of foreshore laminites (Facies 10).

Faunally this sequence may be identified by the first occurrence of the common Permo-Carboniferous genus *Diplognathodus*, represented by *D. coloradoensis* in cycle B9.2. *Neognathodus medexultimus* first appears in the base of cycle B9.3. The last occurrences of pseudostaffellid foraminifera, which range upward from the base of sequence LAI-B5, is found in the upper meter of the sequence at the top of cycle B9.4.

Sequence LAI-B10. The sequence boundary at the base of cycle B10.1 is coincident with the transgressive surface. The transgressive systems tract is comprised of the meter-thick cycle 10.1. Maximum flooding occurs atop this cycle where mixed heterozoan/photozoan skeletal packstones (Facies 5) are overlain by distal outer-ramp Facies 2. Highstand conditions are long-lived consisting of 17 meters (cycles B10.2 to B10.6) of this ~18 meter-thick sequence (~324-ka duration). The abundance of fine-grained eolian siliciclastics significantly increases up section with each cycle comprising the highstand systems tract. The top of cycle B10.6 is capped by a soil horizon, which serves as the capping sequence boundary.

Sequence LAI-B11 (incomplete). Only the first two cycles in this sequence were studied for this project. The base of this sequence is the soil horizon capping sequence LAI-B10. Cycle B11.1, just above the soil, contains three-meters of fine-grained eolian silt (Facies 11), most likely reworked during lowstand conditions. The base of the next cycle (B11.2) contains a succession of transgressive skeletal packstones that initiate the transgressive systems tract.

Sequence LAI-B11 is distinguished by the first occurrences of enlongate fusulinids. *Profusulinells spicata* first occurs in the caprock of cycle B11.2, defining the Morrowan-Atokan boundary.

DISCUSSION

Ramp model during icehouse conditions. As previously mentioned, deposition for the Late Pennsylvanian carbonates of Arrow Canyon occurred under high-amplitude, high-frequency icehouse conditions on a distally steepened carbonate ramp where lagoonal, foreshore, and wave-agitated shoal packstones and grainstones graded without a break in slope to low-energy, outer-ramp wackestones and mudstones. As defined by Ahr (1973), the basic carbonate ramp model is a sloping topographic surface containing concentric facies belts that grade from grainstones to mudstones basinward and follow bathymetric contours; patch reefs may be present locally, but continuous reef trends are absent. The lack of both a shelf break and a continuous reef complex allows the carbonate factory to migrate seaward along a gently sloping ramp rather than completely shutting down with changes in relative sea level (Read, 1998). Read (1998) noted that icehouse ramps tend to have ramp tops with steeper gradients—30 cm/km to >1 m/km—than greenhouse and transitional ramps. These steep ramp tops combined with large changes in eustatic sea level cause icehouse ramp carbonates to continually try to equilibrate to changing water depths (Read, 1998). This, in turn, causes rapid lateral migration of individual depositional environments which produces low carbonate sedimentation rates, resulting in much unfilled accommodation space (Read, 1998). In addition, these low sedimentation rates result in fairly thin, shingled parasequences (Read, 1998). Based on a Fischer diagram of the Morrowan through Desmoinesian cycles of Arrow Canyon and facies stacking patterns (Figures 8), the Morrowan was a time of unfilled accommodation space and shows evidence of rapid lateral facies

migration (i.e., cycles B7.1 to B7.4) and non-Waltherian facies shifts (i.e., cycles B3.7, B4.2 to B5.1).

Additionally, Read (1998) states that tidal flat facies tend to be rare on icehouse ramps because higher slopes encourage more energetic coastal and beach settings and high rates of sea-level fall cause the shoreline to migrate rapidly seaward, which outpaces the progradation of any tidal flat facies and results in disconformities forming directly on subtidal facies. Thus, tidal-flat growth on icehouse ramps is often linked to relative stillstands of sea level, while disconformities tend to be common and well-developed during lowstands and serve as cycle caps because of large changes in sea level and long exposure times (Read, 1998). In the Morrowan Bird Spring Formation, only two of 59 fifth-order cycles contain tidal flat facies (Facies 10). Rather, subaerial exposures and high-energy shoal and foreshore grainstones (Facies 6, 7, 8, and 11) cap 27 of the 59 cycles.

Climatic effects on ramp deposition. The cycles in Arrow Canyon are dominated by carbonates and lacked a proximal source of siliciclastics; however, the presence of fine-grained, sub-rounded to subangular, eolian siliciclastics indicates that climate also may have influenced the deposition of these cycles. Based on insights drawn from her analogy of the Quaternary with the Late Carboniferous and sedimentologic data from the Pedregosa and Orogrande basins, Soreghan (1994) suggests that coupled glacioeustatic and glacioclimatic change influenced Late Carboniferous cyclostratigraphy. During the Carboniferous, Arrow Canyon and the Pedregosa and Orogrande basins were positioned at similar latitudes. Soreghan (1994) noted that this latitudinal zone likely experienced significant glacial-interglacial climatic shifts; namely, this region would have

experienced intensified aridity and intensified humidity during extremes of glacial and interglacial climate, respectively. During icehouse times, atmospheric Hadley cells contract (Figure 11) and the tropical humid belt shrinks, allowing a broad arid belt to develop (Read et al., 1995; Soreghan, 1994). This shrinkage of Hadley cells also can allow temperate, more humid regions to develop in previously arid regions (Read et al., 1995; Soreghan, 1994). Drawing evidence from Quaternary studies that trade wind intensities may have increased by 20 to 50% during glacial-phases, Soreghan (1994) suggests that similar increases could have occurred during the Late Carboniferous. This climate-induced aridity and increase in wind intensities during glacial phases may explain the increase of eolianites in the upper half of the Morrowan section (particularly from cycle B10.2 upward). These eolian silts have been categorized based on faunal composition as distal-outer ramp facies. However, they appear in the upper portions of cycles where one would expect to see shallower facies. It seems that these silts were abundant enough to prevent the shallow-water carbonate factory from fully developing, thus, inducing heterozoan association conditions in shallow, inner-ramp waters.

CONCLUSIONS

Section completeness, quality of exposure, and near continuous deposition of the Bird Spring Formation along a carbonate ramp, located in present-day Arrow Canyon, Nevada, allowed for detailed sampling of the Morrowan portion of the Lower Absaroka Ia supersequence. Compositional data obtained from quantitative analysis of 333 of 345 petrographic thin sections produced cluster analyses, which formed the basis for twelve facies associations: three heterozoan distal outer-outer ramp facies, three heterozoan to

transitional proximal outer-ramp facies, five photozoan inner-ramp facies, and one lowstand mixed siliciclastic-carbonate facies. Facies stacking patterns combined with outcrop data yielded 59 fifth-order fundamental cycles, which stacked into ten third-order sequences. Changes in both cycle thickness and fundamental cycle types indicate that the second-order sea-level curve of Golonka and Keissling (2002) for the Lower Absaroka Ia supersequence should be modified to reflect (1) rising seas from shortly before the Mid-Carboniferous boundary, (2) maximum flooding conditions in cycle LAI-B6.1 (horizons A-135 to A-145—120 to 135 meters above the Mid-Carboniferous boundary), and (3) falling seas from cycle LAI-B6.1 to the top of cycle LAI-B10.6 (between horizons A-218 to A-219) which lies ~6 meters below the Morrowan-Atokan boundary.

REFERENCES

Ahr, A.M., 1973, The carbonate ramp: An alternative to the shelf model: Gulf Coast Association of Geological Societies, v.23, p. 221-25.

Amoco Production Company, unpublished, Micropaleonotology data of the Arrow Canyon, Clark County, Nevada, measured section.

Beauchamp, B., 1994, Permian climatic cooling in the Canadian Arctic: Geological Society of America, Special Paper 288, p. 229-46.

Beauchamp, B., and Baud, A., 2002. Growth and demise of Permian biogenic chert along northwest Pangea: Evidence for end-Permian collapse of thermohaline circulation: Palaeogeography, Palaeoclimatology, Palaeoecology, v. 184, p. 37-63.

Blakey, R. C., 1997, Pennsylvanian Paleogeography, Southwestern US, http://jan.ucc.nau.edu/~rcb7/penpaleo.html.

Burchette, T. P., and Wright, V. P., 1992, Carbonate ramp depositional systems: Sedimentary Geology, v. 8, p. 67-115.

Cassity, P. E., and Langenheim, R. L., Jr., 1966, Pennsylvanian and Permian fusulinids of the Bird Spring Group from Arrow Canyon, Clark County, Nevada: Journal of Paleontology, v. 40, p. 931-968.

Dennison, J. M., and Shea, J. H., 1966, Reliability of visual estimates of grain abundance: Journal of Sedimentary Petrology, v. 36, n. 1, p. 81-89.

Flügel, E., 1982, Microfacies analysis of limestones: Springer-Verlag, New York, 633 p.

Giles, K. A., 1996, Tectonically forced retrogradation of the lower Mississippian Joana Limestone, Nevada and Utah, *in* Longman, M. W., and Sonnenfeld, M. D. (eds.), Paleozoic systems of the Rocky Mountain region: Society for Sedimentary Geology, p. 145-164,

Golonka, J., 2002, Plate-tectonic maps of the Phanerozoic: Society for Sedimentary Geology, Special Publication No. 72, p. 21-75.

Golonka, J., and Kiessling, W., 2002, Phanerozoic time scale and definition of time slices: Society for Sedimentary Geology, Special Publication No. 72, p. 11-20.

Groves, J. R., Nemyrovska, T. I., and Alekseev, A. S., 1999, Correlation of the type Bashkirian Stage (Middle Carboniferous, South Urals) with the Morrowan and Atokan Series of the Midcontinental and Western United States: Journal of Paleontology, v. 73, n. 33.

Halfar, J., Godinez-Orta, L., and Ingle, J. C., Jr., 2000, Microfacies analysis of recent carbonate environments in the southern Gulf of California, Mexico—A model for warm-temperate to subtropical carbonate formation: Palaios, v. 15, p. 323-342.

Heath, C. P., Lumsden D. N., and Carozzi, A. V., 1967, Petrography of a carbonate transgressive-regressive sequence: The Bird Spring Group (Pennsylvanian), Arrow Canyon Range, Clark County, Nevada: Journal of Sedimentary Petrology, v. 37, p. 377-400.

James, N. P., 1997, The cool-water carbonate depositional realm: Society for Sedimentary Geology Special Publication, v. 56, p. 1-20.

Khaiwka, M. H., El-Sayed, M. I. A., and Al-Shamlan, A. A., 1987, The utility of cluster analysis in determining sedimentary facies, Sedimentary Geology, v. 30, n. 4, p. 245-253.

Lees, A. and Buller, A. T., 1972, Modern temperate-water and warm-water shelf carbonate sediments contrasted: Marine Geology, n. 13, p. 67-73.

Langenheim, V. A. M., and Langenheim, R. L., Jr., 1965, The Bird Spring Group, Chesterian through Wolfcampian, at Arrow Canyon, Arrow Canyon Range, Clark County, Nevada: Illinois Academy of Science Transactions, v. 57, p. 225-240 .

Leavitt, A. J., 2002, Stratigraphic architecture of mid-ramp, icehouse carbonates: A case study from Desmoinesian strata (Middle Pennsylvanian) of Arrow Canyon, Southern Nevada: Brigham Young University M.S. Thesis, 52 p.

Lehrmann, D. J., and Goldhammer, R. K, 1999, Secular variation in facies and parasequence stacking patterns of platform carbonates: a guide to application of the stacking patterns technique in strata of diverse ages and settings, *in* Harris, P. M., et al. (eds.), Recent Advances in carbonate sequence stratigraphy; applications to reservoirs, outcrops and models: Society for Sedimentary Geology, Special Publication No. 63, p. 187-226.

Lumsden, D. N., 1965, Microfacies of the middle Bird Spring Group (Pennsylvanian-Permian), Arrow Canyon Range, Clark County, Nevada: Unpublished Ph.D. thesis, Illinois University, 102 p.

Nowak, F. J., 1972, Microfacies of the upper Bird Spring Group (Pennsylvanian-Permian), Arrow Canyon Range, Clark County, Nevada: University of Illinois Dissertation, 66 p.

Nowak, F. J., and Carozzi, A. V., 1973, Microfacies of the upper Bird Spring Group (Pennsylvanian –Permian), Arrow Canyon Range, Clark County, Nevada: Archive des Science, v. 25, n. 3, p. 343-382.

Pierce, R. W., and Langenheim, R. L., Jr., 1974, Platform conodonts of the Monte Cristo Group, Mississippian, Arrow Canyon Range, Clark County, Nevada: Journal of Paleontology, v. 48, p. 149-169.

Read, J. F., Kerans, C., Weber, L. J., Sarg, J. F., and Wright, F. M., 1995, Milankovitch sea-level changes, cycles, and reservoirs on carbonate platforms in greenhouse and ice-house worlds: Society of Sedimentary Geology, Short Course No. 35.

Read, J. F., 1998, Phanerozoic carbonate ramps from greenhouse, transitional and ice-house worlds: clues from field and modeling studies, *in* Wright, V.P., and Burchette, T.P. (eds.) Carbonate Ramps: Geological Society, London, Special Publication 149, p. 107-135.

Rice, C. L., Belkin, H .E., Henry, T. W., Zartman, R. E., and Kunk, M. J., 1994, The Pennsylvanian Fire Clay tonstein of the Appalachian Basin—Its distribution, biostratigraphy and mineralogy, *in* Rice, C. L. (ed.), Elements of Pennsylvanian stratigraphy, central Appalachian Basin: Geological Society of America, Special Paper, p. 87-104.

Rich, M., 1961, Stratigraphic section and fusulinids of the Bird Spring formation near Lee Canyon, Clark County, Nevada: Journal of Paleontology, v. 35, n. 6, p. 1159-1180.

Ross, C. A., and Ross, J. R. P., 1985, Late Paleozoic depositional sequences are synchronous and worldwide: Geology, v. 13, p. 194-197.

Ross, C. A., and Ross J. R. P., 1987, Late Paleozoic sea levels and depositional sequences: Cushman Foundation for Foraminiferal Research, Special Publication 24, p. 137-149.

Ross, C. A., and Ross, J. R. P., 1988, Late Paleozoic transgressive–regressive deposition, *in* Wilgus, C. K., et al. (eds.), Sea-level changes: An integrated approach: Society of Economic Paleontologists and Mineralogists, Special Paper No. 42, p. 227–247.

Simmons, M., 2004, RE: paleonet Global sea-level curve: http://jerwood.nhm.ac.uk/archives/paleonet/2003/msg00756.html.

Smosna, R., Bruner, K. R., and Burns, A., 1999, Numerical analysis of sandstone composition, provenance, and paleogeography: Journal of Sedimentary Research, v. 69, n. 5, p. 1063-1070.

Sonnenfeld, M. D., 1996, Sequence evolution and hierarchy within the lower Mississippian Madison Limestone of Wyoming *in* Longman, M. W., and

Sonnenfeld, M. D. (eds.), Paleozoic systems of the Rocky Mountain region: Society for Sedimentary Geology, p. 165-192.

Soreghan, G. S., 1994, The impact of glacioclimatic change on Pennsylvanian cyclostratigraphy, *in* Embry, A.F., Beauchamp, B., and Glass, D.J. (eds.), Pangea: global environments and resources: Canadian Society of Petroleum Geologists, Memoir 17, p. 523-543.

Soreghan. G. S., and Giles, K. A., 1999, Amplitudes of late Pennsylvanian glacioeustasy: Geology, v. 27, p. 255-258.

Stevens, C. H., Stone, P., and Ritter, S. M., 2001, Conodont and fusulinid biostratigraphy and history of the Pennsylvanian to Lower Permian Keeler Basin, East-Central California: Brigham Young University Geologic Studies, v. 46, p. 99-142.

Van der plas, L., 1965, In defense of point counting analysis, a reply: Sedimentology, v. 4, p. 247-253.

Webster, G., D., 1969, Chester through Derry conodonts and stratigraphy of northern Clark and southern Lincoln Counties, Nevada: University of California Publications in Geological Sciences, v. 79, p. 1-121.

Webster, G. D., and Lane, N. G., 1967, Mississippian-Pennsylvanian boundary in southern Nevada, *in* Teichert, C., and Yochelson, E. L. (eds.), Essays in Paleontology and Stratigraphy, R.C. Moore Commemorative Volume: Department of Geology: University of Kansas, Special Publication 2, p. 502-529.

Westphal, H., Reijmer, J. J. G., and Head, M. J., 1999, Input and diagenesis on a carbonate slope (Bahamas): Response to morphology evolution and sea-level fluctuations, *in* Harris, P. M., Saller, A., and Simo J. A., Advances in Carbonate Sequence Stratigraphy: Applications to Reservoirs, Outcrops, and Models: Society for Sedimentary Geology, Special Publication 63, p. 247-274.

Young, G. C., and Laurie, J. R. (eds.), 1995, An Australian Phanerozoic timescale: Oxford University Press, 279 p., 12 charts.

Zempolich, W. G., and Erba, E., 1999, Sedimentologic and chemostratigraphic recognition of third-order sequences in resedimented carbonate: The Middle Jurassic Vajont Limestone, *in* Harris, P. M., Saller, A. H., and Simo, J. A. (eds.), Advances in Carbonate Sequence Stratigraphy: Application to Reservoirs, Outcrops and Models: Society for Sedimentary Geology, Special Publication 63, p. 335–370.

	Facies 0 Laminated mudstone facies	**Facies 1** Burrowed mudstone to sparse wackestone facies	**Facies 2** Heterozoan skeletal wackestone facies	**Facies 3** Transgressive skeletal packstone facies	**Facies 4** Over-packed crinoid packstone facies	**Facies 5** Mixed heterozoan/ photozoan wackestone to grain-dominated packstone facies
Photozoan vs. heterozoan	Heterozoan	Heterozoan	Heterozoan	Heterozoan to transitional	Heterozoan to transitional	Heterozoan to transitional
Texture & lithology	- Dark gray mudstone - Silty mudstone	- Dark gray to silty mud-wackestones - Abundant chert lenses	- Wackestone to mud-dominated packstone	- Over-packed packstone due to pervasive compaction	- Over-packed packstone	- Wackestone to grain-dominated packstone
Sedimentary structures	- mm-thick laminae - Rare burrowing (cf. *Zoophycus*)	- Massive bedding with lenticular to modular chert - Rare burrows filled with sponge spicules	- Medium to thick bedding with nodular and lenticular chert - cm-scale burrows	- Weathers to slopes - Platy	- Massive to thick bedding	- Graded tempestites and hummocky cross-stratification destroyed by bioturbation
Composition*	- Mud: 65-91% - Quartz silt (10-50 µm diameter, subangular): 10-30% - Microbioclasts	- Mud: 54-98% - Silt-sized microbioclasts: 2-30% - Quartz silt (20-30 µm diameter, subangular): 5-10% - Rare crinoid columnals, disarticulated brachiopods, and other skeletal grains	- Dense micrite mud - Whole fossils - Rich in heterozoan invertebrate fauna: crinoids, spiriferid and productid brachiopods, fenestrate and twiggy bryozoan, sponge spicules, sparse rugose coral, rare trilobites - Microbioclasts	- Dark gray to black organic rich mud - Whole to broken brachiopods: up to 65% - Disarticulated crinoid columnals: up to 59% - Minor heterozoan skeletal components - Irregular phosphate grains	- Whole to abraded crinoid columnals: up to 64% - Minor amounts: brachiopod and bryozoan debris - Minor heterozoan skeletal components - Occasional small foraminifera	- Medium- to coarse-sand sized heterozoan skeletal grains - Muddy matrix with microbioclasts - Quartz silt: 0-15% - When present, photozoan components: 15-20% - Many samples contain a variety of small foraminifera
Significant diagenetic features		- Silicification	- Silicification - Some microspar and pseudospar - Oriented grains	- Oriented and sutured grains - Phosphatization - Some microspar	- No meteoric diagenesis - Sutured and penetrative grain contacts	
Depositional environment	- Distal outer ramp - Below swb - Anaerobic - Storm suspension - Gravity flows	- Distal outer ramp - Below swb - Dysaerobic - Storm suspension - Gravity flows	- Distal outer ramp - Below swb - Well-oxygenated - Subphotic	- Proximal outer ramp - Fwwb to swb - Slow deposition during rapid sea-level rise	- Proximal outer ramp - Fwwb and swb	- Proximal outer ramp - Fwwb and swb - Increase in ambient light - Sediment gravity flows
% of section (in meters)§	2.9%	13.2%	14.5%	2.5%	0.9%	33%
% of caprock units (in no.)**	0%	0%	0%	0%	1.7%	28.8%
% of base rock units (in no.)**	3.4%	5.1%	16.9%	10.2%	0%	33.9%

Table 1. Facies Descriptions.

§ Soils comprise 0.4% of the section, and 8.3% is unknown because it is covered or too difficult to sample.

* Heterozoan skeletal components include brachiopods, crinoids, echinoids, bryozoans, trilobites, ostracodes, conodonts, inarticulate brachiopods.

** Sampling was not always possible; thus, some base rock and caprock facies are unknown. Soil horizons composed 5.2% of caprock facies.

	Facies 6 Oncoidal packstone to grainstone facies	**Facies 7** High-energy shoal grainstone facies	**Facies 8** High-energy laminated foreshore facies	**Facies 9** Lagoonal packstone to grainstone facies	**Facies 10** Peritidal laminite facies	**Facies 11** Mixed siliciclastic-carbonate facies
Photozoan vs. heterozoan	Photozoan	Photozoan	Photozoan	Photozoan	Photozoan	Siliciclastic/ Photozoan
Texture & lithology	- Dominantly packstones - Some oncoidal wackestones to grainstones	- Skeletal grain-dominated packstones to grainstones	- Grain-dominated packstone layers interbedded with muddy layers or quartz-rich layers	- Dark gray mud-dominated packstones to grainstones	- Fine-grained packstones to grainstones with muddy lenses	- Quartz grain-dominated packstones to grainstones
Sedimentary structures	- Blocky ledge - Some cross-bedding	- Cross-bedding	- Planar lamination to low-angle cross-bedding	- Massive to thin bedding - Some burrowing	- Fine-scale upward grading laminae - Muddy lenses	- Cross-bedding
Composition*	- Oncoids: up to75% - Mud: up to 53% - Skeletal grains: heterozoan skeletal debris, whole to broken gastropods, bivalve fragments, coiled and irregular foraminifera calcareous algae—all may also serve a oncoid nuclei - Micrite rims - Non-skeletal grains: ooids, superficial ooids, peloids, intraclasts, small to moderate amounts of silt	- Grains are finely comminuted, rounded, micritized - Crinoids: up to 79% - Brachiopods: up to 43% - Bryozoans: up to 29% - Minor molluscs, microbioclasts, coated grains, phosphatics, trilobites, ostracods, algae, intraclasts, peloids, phosphatics, and small foraminifera	- Composition varied with availability of material from the adjacent ramp crest - Peloids interbedded with mud - Oncoid interbedded with peloids - Silt-size quartz grains interbedded with oncoids-rich	- Peloids: up to 27% - Mud: up to 63% - Coated grains: up to 34% - Microbioclasts: up to 39% - Heterozoan skeletal grains - Lesser amounts of quartz grains; molluscs; small, irregular, and/or large forams; calcispheres; intraclasts - Frequently, skeletal grains and microbioclasts are rounded, micritized and/or have oolitic coatings	- Composition varied between cycles - Silt-size microbioclastic and peloidal fining-up layers - Muddy layers interbedded with oncoids and skeletal debris	o Quartz grains (subangular to sub-rounded, 50-200 µm diameter): up to 84% o Mud: 10-57% o Bioclasts include heterozoan skeletal fragments, microbioclasts, molluscs, algae, and a few small and/or irregular forams
Significant diagenetic features		- Sparry calcite cement (meteoric diagenesis) - Sutured grains				-Fused grains
Depositional environment	- Inner ramp crest - Above fwwb - Moderate- to high-energy	- Inner ramp crest - Above fwwb - High-energy shoal	- Inner ramp beach - High-energy foreshore	- Inner ramp lagoon - Restricted - Subtidal	- Inner ramp tidal flat	- Eolian transport of silt grains to exposed ramp - Reworked on inner ramp
% of section (in meters) §	7.1%	5%	2.9%	6.9%	0.5%	1.9%
% of caprock units (in no.)**	16.9%	16.9%	8.5%	15.3%	1.7%	1.7%
% of base rock units (in no.)**	1.7%	1.7%	5.2%	3.4%	0%	1.7%

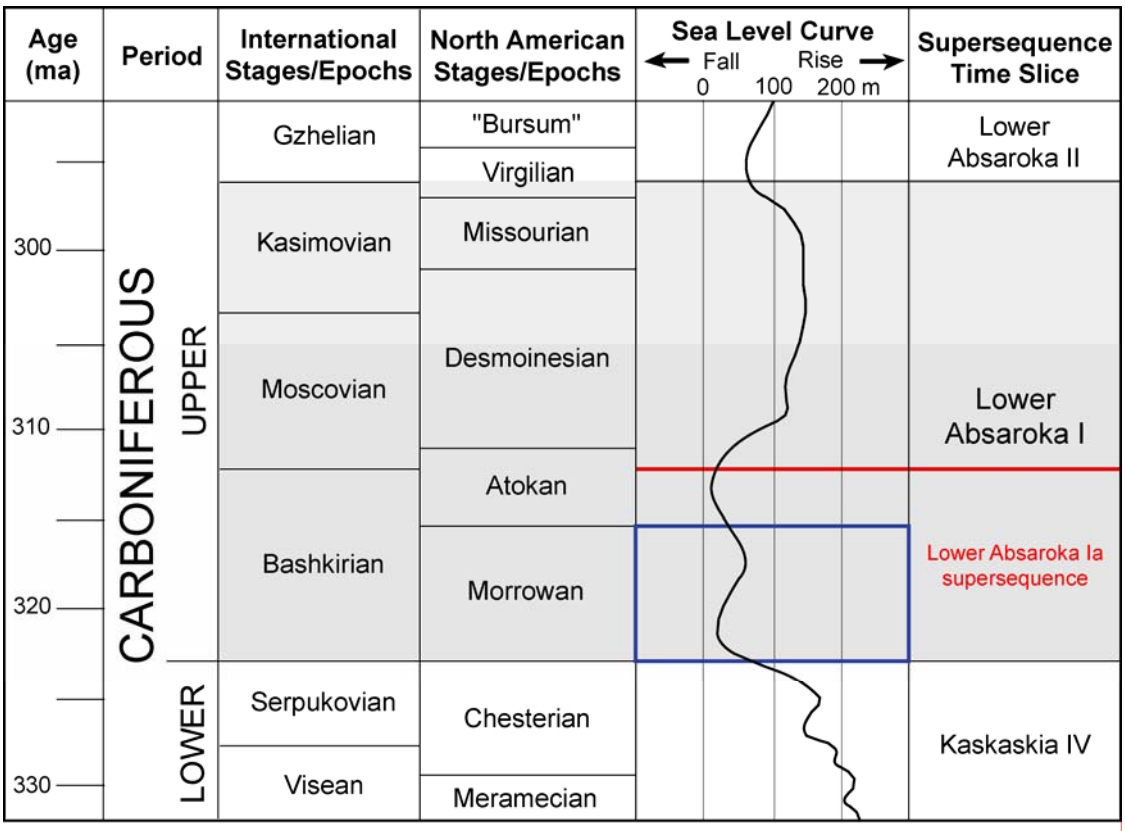

Figure 1. Chronostratigraphic framework and sea-level curve of the Lower Absaroka I time slice after Golonka and Keissling (2002). The red line denotes the top of the second-order Lower Absaroka Ia supersequence. The blue box shows the Morrowan portion studied for this project.

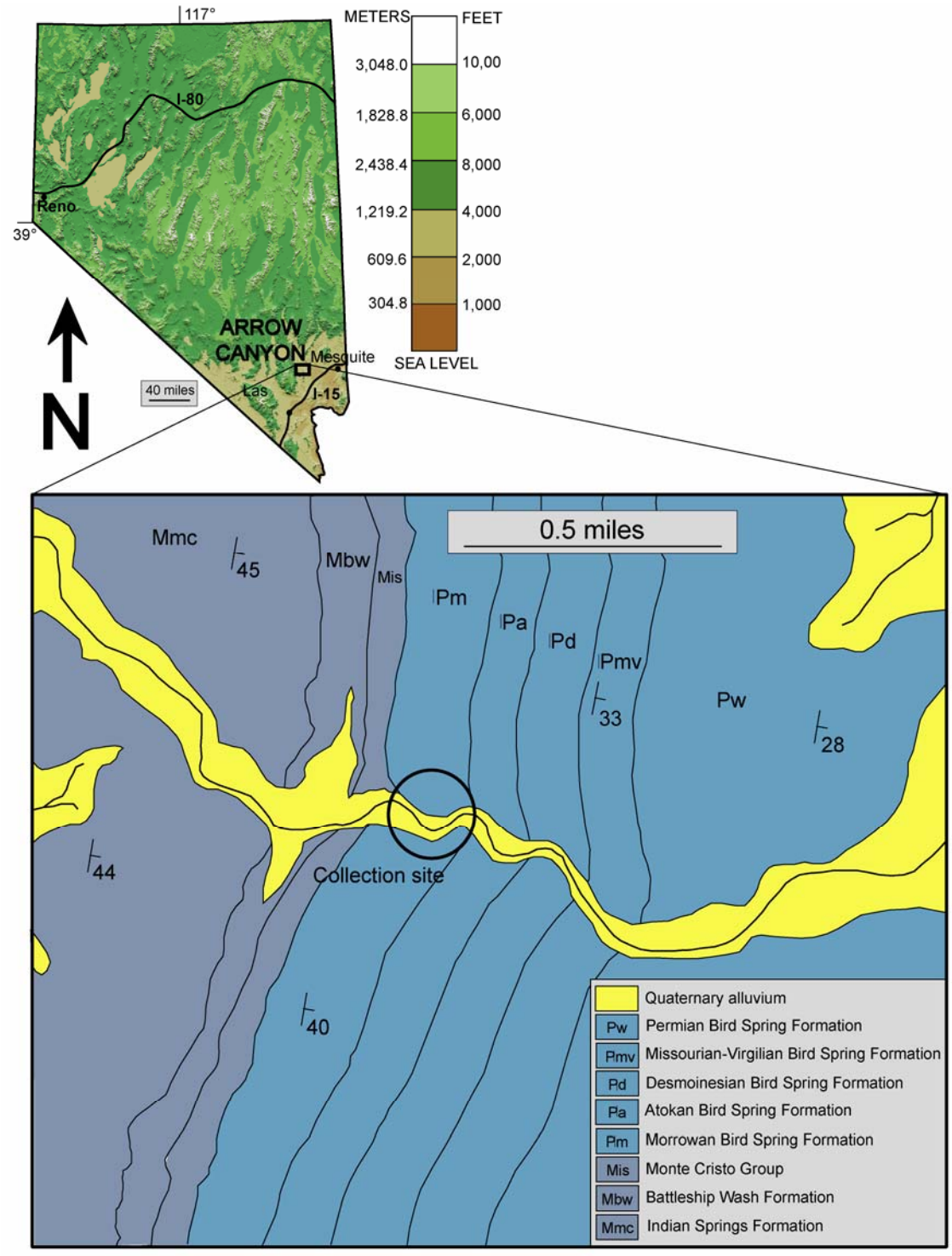

Figure 2. Geologic locality map of Arrow Canyon, Clark County, Nevada, showing Carboniferous and Permian formations (adapted from and http://wwwflag.wr.usgs.gov/USGSFlag/Data/maps/NevadaDEM.html).

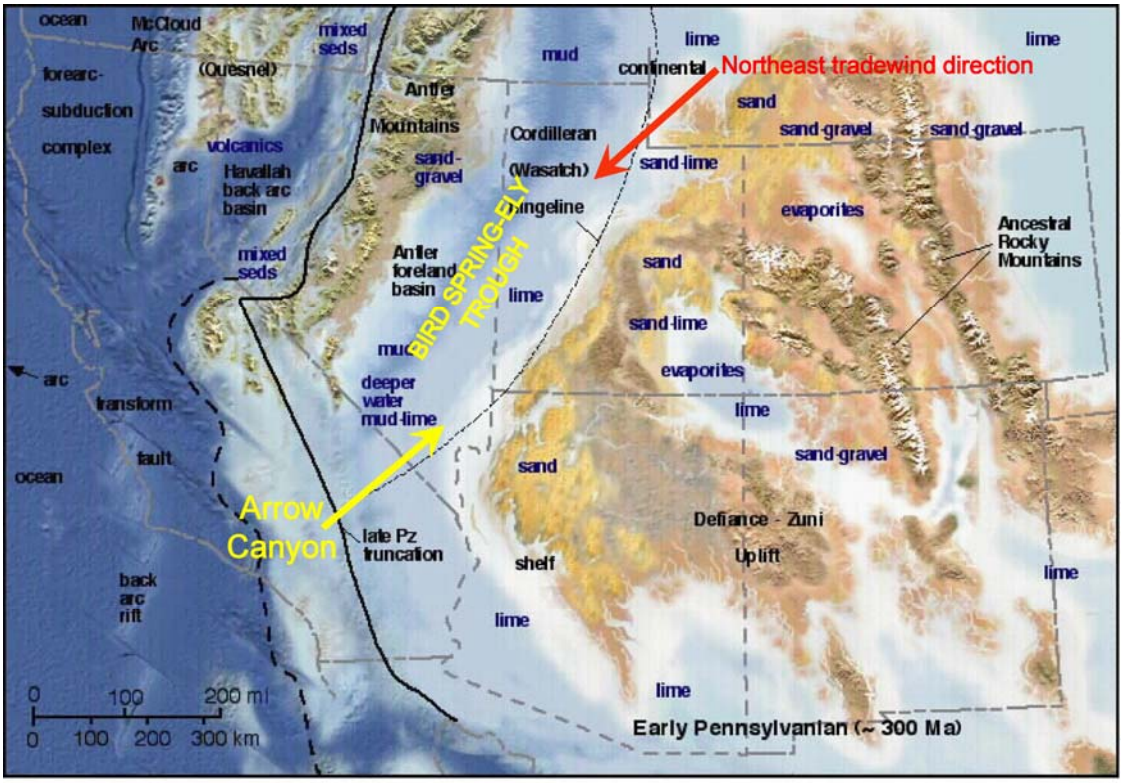

Figure 3. Paleogeography of southwestern North America during the Late Carboniferous showing location of Bird Spring-Ely trough and present-day Arrow Canyon (adapted from Blakey, 1997).

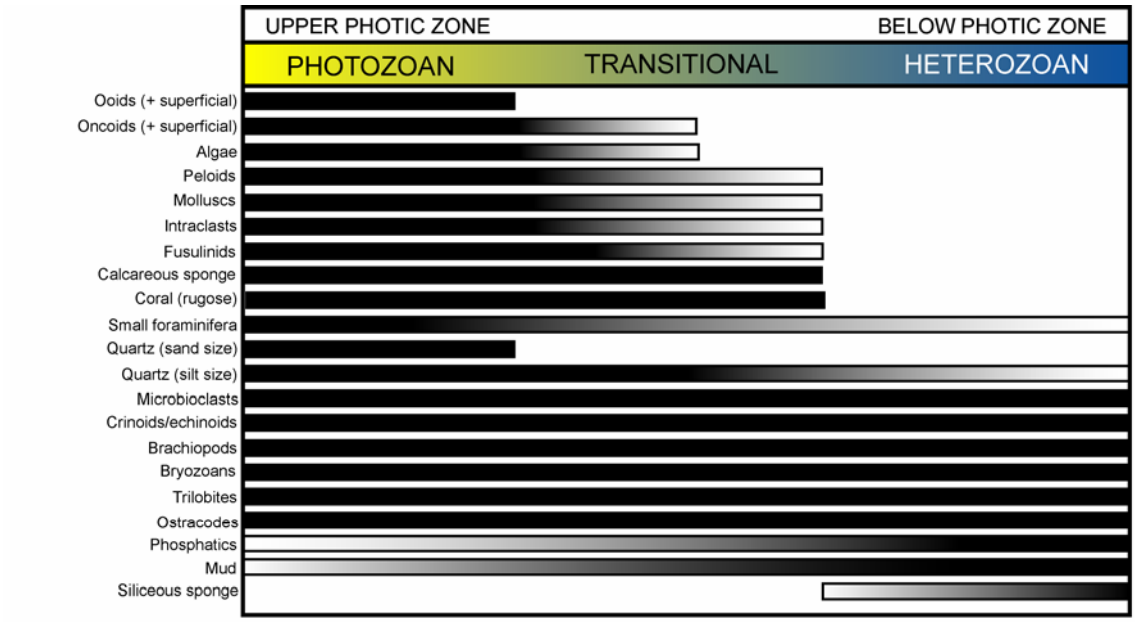

Figure 4. Ecological ranges of skeletal and non-skeletal components comprising the Morrowan Bird Spring succession. Bars represent the sediment association, photozoan or heterozoan, to which the components belong. Dark regions = potential abundance; light regions = minor amounts.

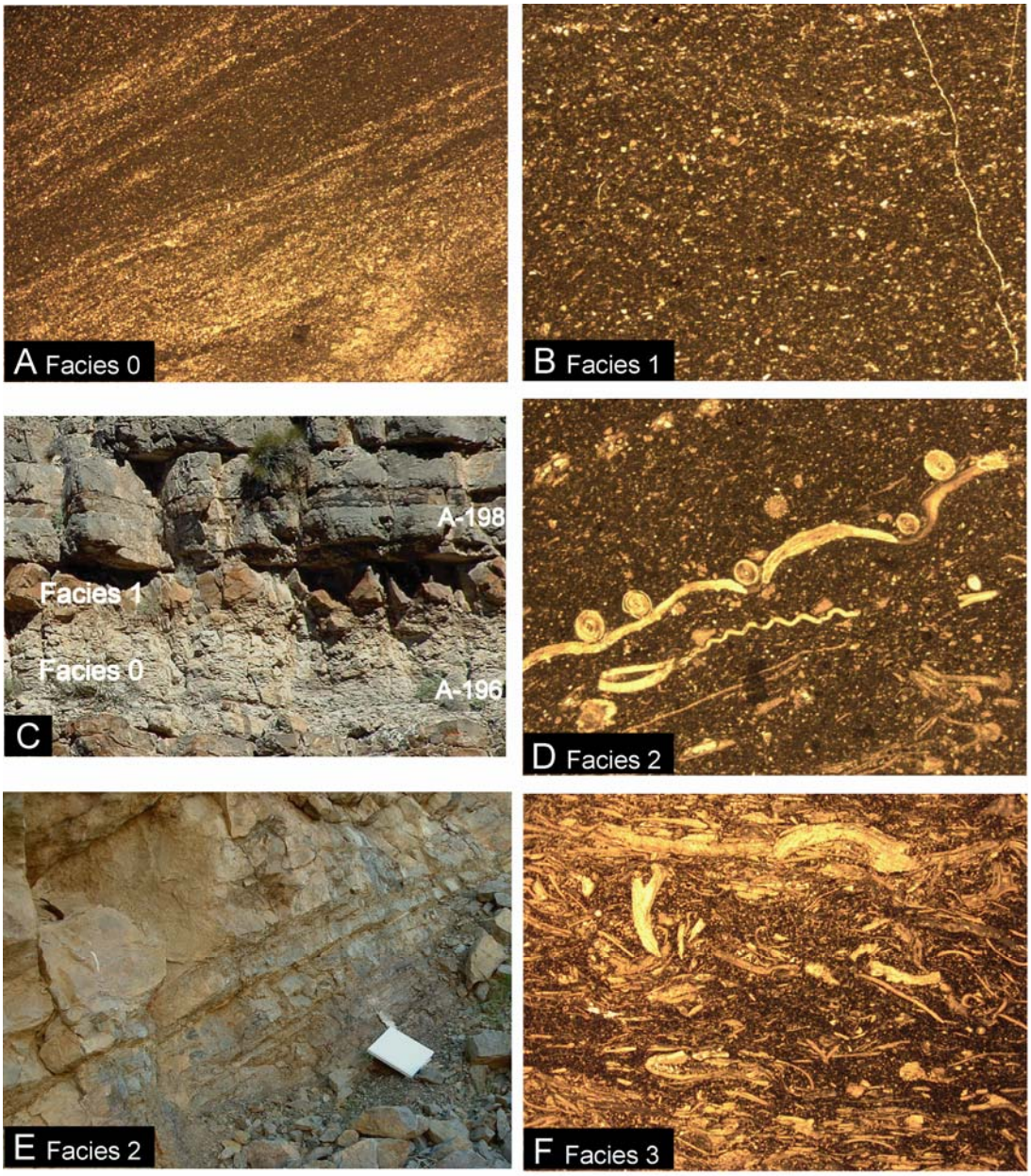

Figure 5. **(A)** Facies 0 (sample M-36B, 1x magnification) is laminated and contains rare fossil fragments, indicating deep-water deposition. **(B)** Facies 1 (sample M-26F, 2x magnification) is similar to Facies 0, but is massive and lacks lamination. **(C)** Facies 0 (white band) and 1 (orange band) outcrop located from A-195.5 through A-198 (samples M-41A-E). **(D)** Facies 2 (sample M-3D, 2x magnification) contains whole fossils and microbioclasts, reflecting outer-ramp deposition under well-oxygenated, low energy, subphotic conditions. **(E)** Facies 2 outcrop at A-91 (samples M-17A). It is frequently found at the base of deep subtidal cycles. **(F)** Facies 5 (sample M-22B, 1x magnification) contains abundant oriented brachiopods, indicating slow sedimentation rates during rapid sea-level rise.

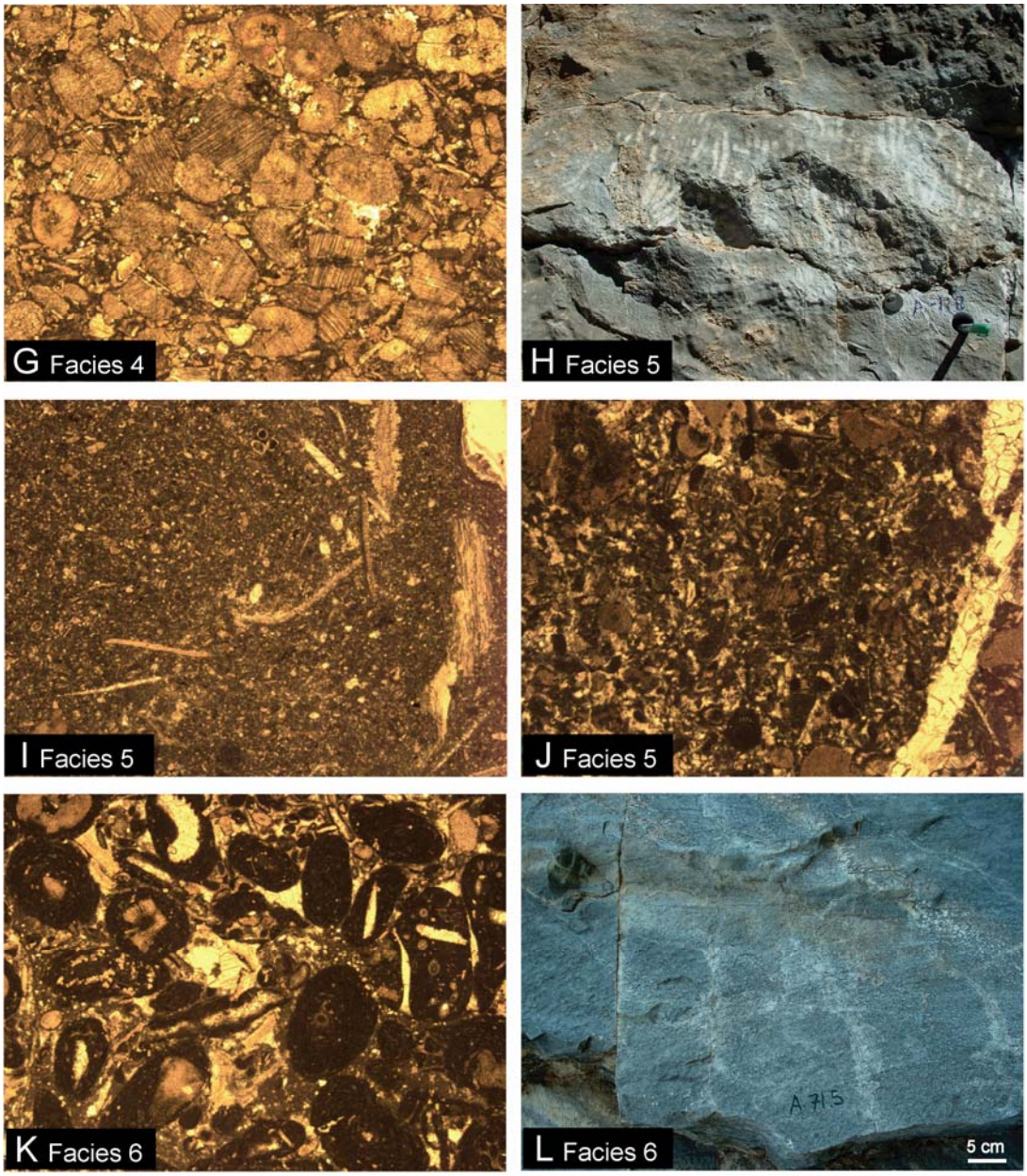

Figure 5. **(G)** Facies 4 (sample M-8I, 2x magnification) represents deposits of abundant crinoid meadows in moderately deep water below fair weather wave base. **(H)** Facies 5 outcrop at A-118 (sample M-22M) of rugose corals beds in a muddy matrix. Coral beds were rare in this section, and most are found in samples categorized as Facies 5. **(I)** Facies 5 (sample M-7D, 2x magnification) is dominated by heterozoan skeletal grains but may contain photozoan components. This sample lacks photozoan sediments. **(J)** Sample M-7F (2x magnification) is an example of Facies 5 containing 9% photozoan components. **(K)** Facies 6 (sample M-5B, 2x magnification) is dominated by oncoids and represents shallow-water deposition. **(L)** Facies 6 outcrop at A-71.5 (sample M-6E/F) contains cross-bedded oncoids; the abundant white specks are the *Girvanella* algal coatings of the oncoids.

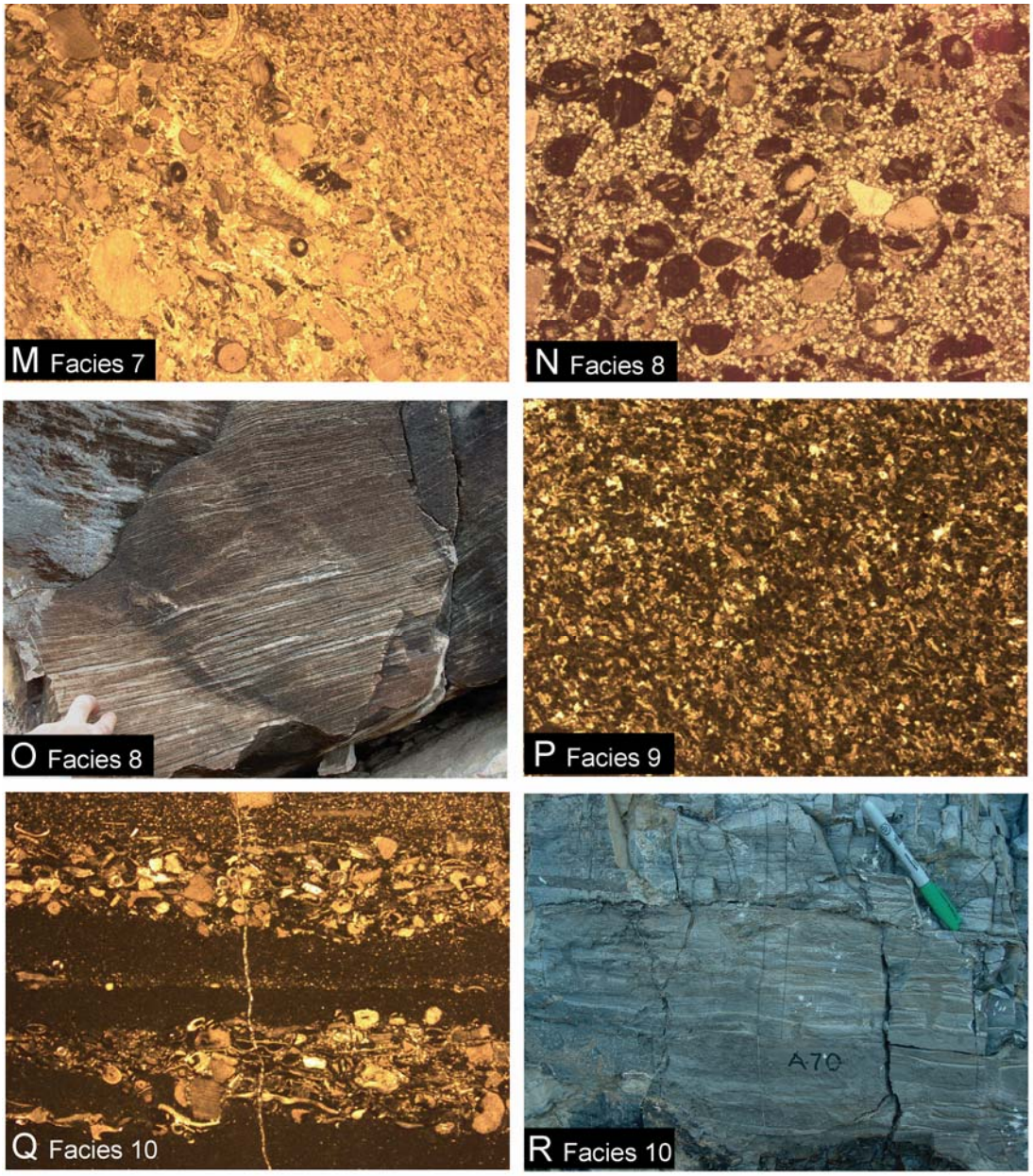

Figure 5. **(M)** Facies 7 (sample M-18J, 1x magnification) is typically cross-bedded and represents a high-energy, shallow-water skeletal shoal environment. **(N)** Facies 8 (sample M-34BC, 2x magnification) is laminated or contains low angle cross-beds, representing deposition along a high-energy foreshore beach. **(O)** Outcrop of sample M-34BC (Facies 8) at A-167. **(P)** Facies 9 (sample M-20L, 2x magnification) is distinguished by an abundance of peloids, finely commuted, rounded, micritized skeletal grains and microbioclasts, representing deposition in a shallow, restricted lagoon environment. **(Q)** Facies 10 (sample M-6C, 1x magnification) represents tidal flat deposition. Peritidal laminites are rare and found only in cycles LA-B1.1 and LAI-B1.7. **(R)** Outcrop of Facies 10 (sample M-6C/D) at A-70.

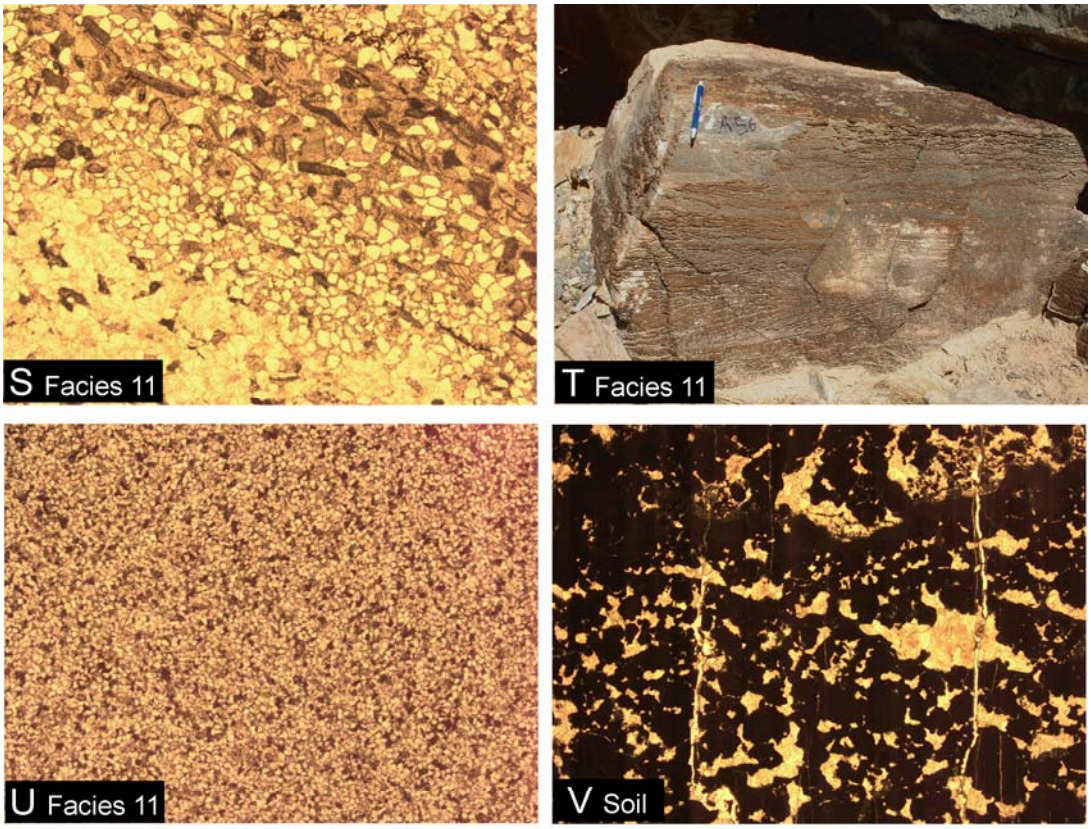

Figure 5. **(S)** Facies 11 (sample M-2A', 2x magnification) contains predominantly sand-sized, subangular to sub-rounded quartz bedded with lenses of rounded, micritized skeletal grains, representing the reworking of eolian sands during third-order lowstand conditions. This sample occurs 2.5 meters above the base of the mid-Carboniferous boundary. **(T)** Outcrop of Facies 11 at A-56 (sample 2A'-B). **(U)** Sample M-49D (2x magnification) is a finer grained variety of Facies 11 and occurs just below the base of the Morrowan-Atokan boundary. **(W)** Soil horizons (sample M-6D, 1x magnification) are rare in this section. When present, they cap cycles.

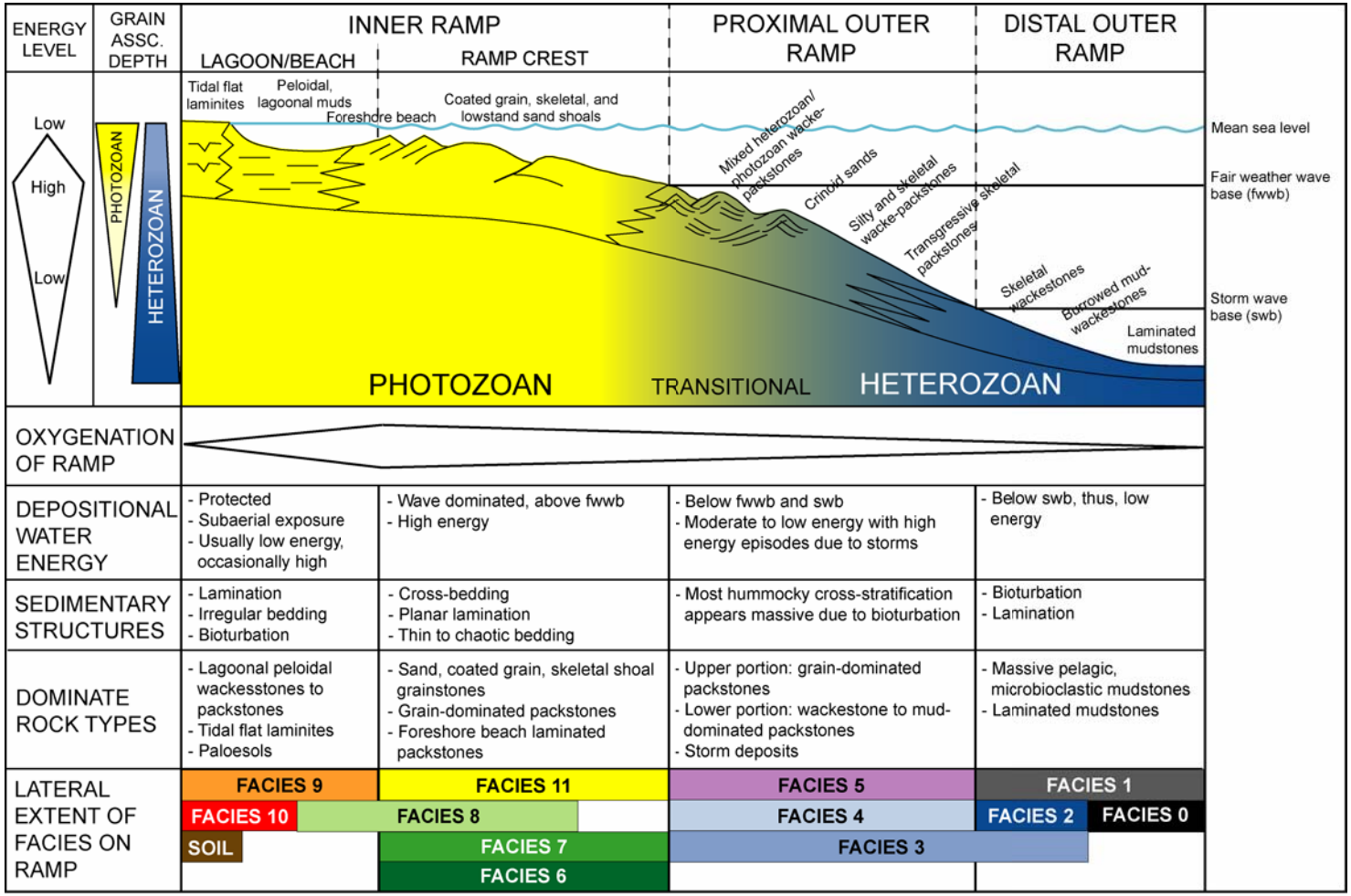

Figure 6. Carbonate ramp model for the Morrowan Bird Spring strata in Arrow Canyon, Nevada (ramp profile adapted from James, 1997). As water depth increases, energy levels, oxygenation, and ambient light decrease. The carbonate factory creating photozoan sediments gradually disappears and muddy heterozoan sediments dominate the outer ramp.

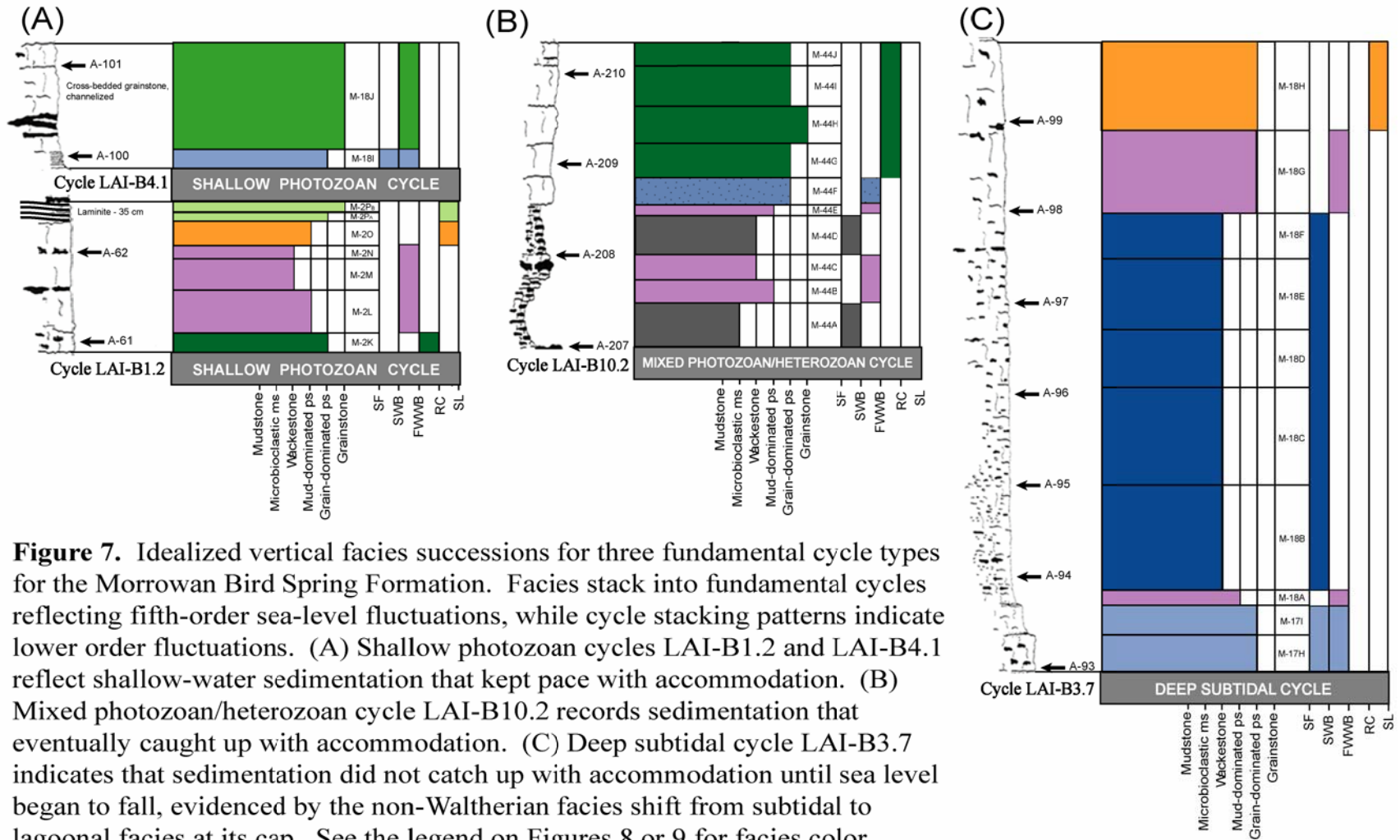

Figure 7. Idealized vertical facies successions for three fundamental cycle types for the Morrowan Bird Spring Formation. Facies stack into fundamental cycles reflecting fifth-order sea-level fluctuations, while cycle stacking patterns indicate lower order fluctuations. (A) Shallow photozoan cycles LAI-B1.2 and LAI-B4.1 reflect shallow-water sedimentation that kept pace with accommodation. (B) Mixed photozoan/heterozoan cycle LAI-B10.2 records sedimentation that eventually caught up with accommodation. (C) Deep subtidal cycle LAI-B3.7 indicates that sedimentation did not catch up with accommodation until sea level began to fall, evidenced by the non-Waltherian facies shift from subtidal to lagoonal facies at its cap. See the legend on Figures 8 or 9 for facies color coding. (SL = sea level, RC = ramp crest, FWWB = fair weather wave base, SWB = storm wave base, SF = sea floor.)

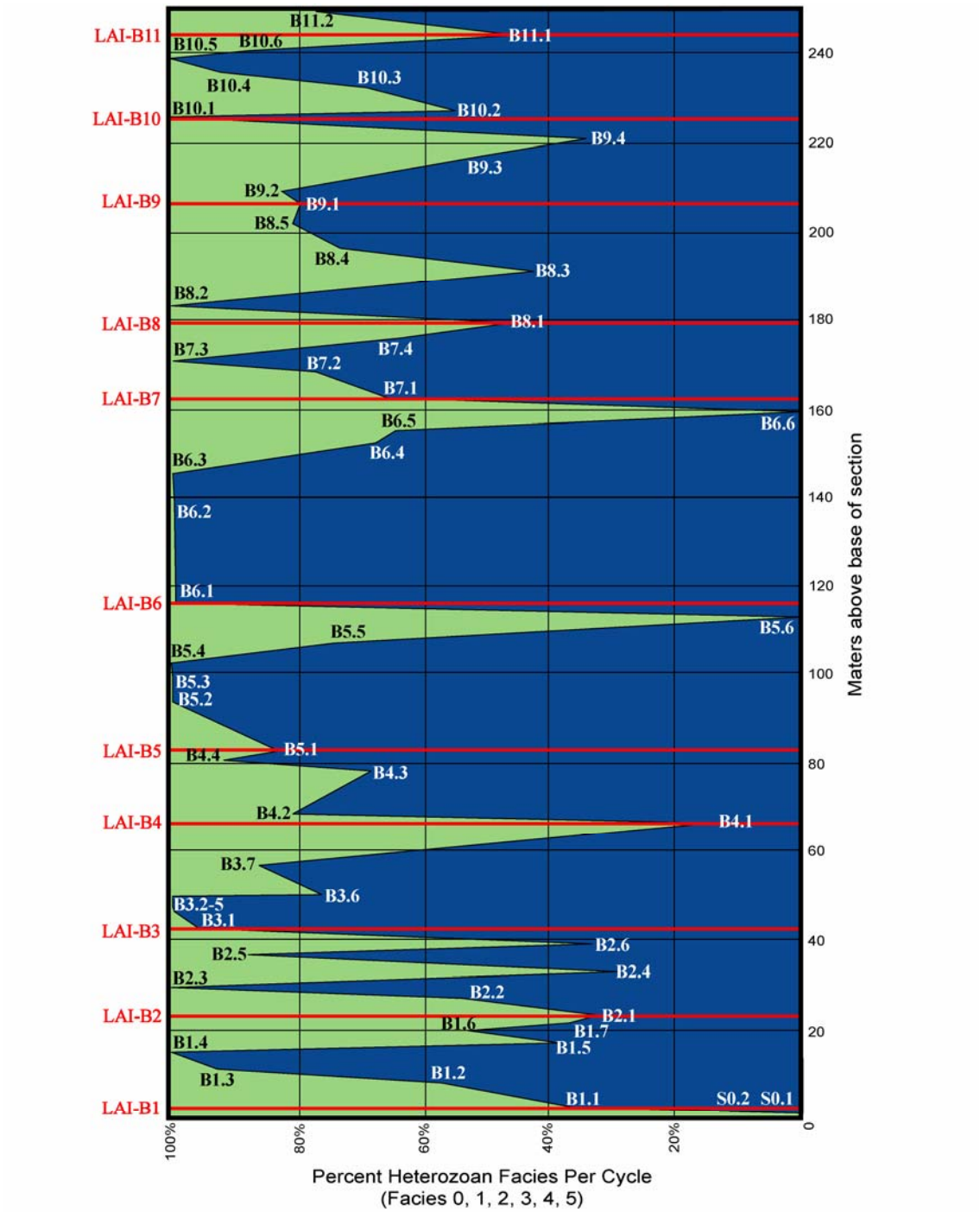

Figure 10. Relative abundance curve of heterozoan versus photozoan facies per cycle. The bases of 59 fifth-order cycles are plotted according to their stratigraphic position above the base of the section (meters). Cycles dominated by heterozoan facies (high percentage) plot on the left side of the graph. The red labels mark third-order sequence boundaries.

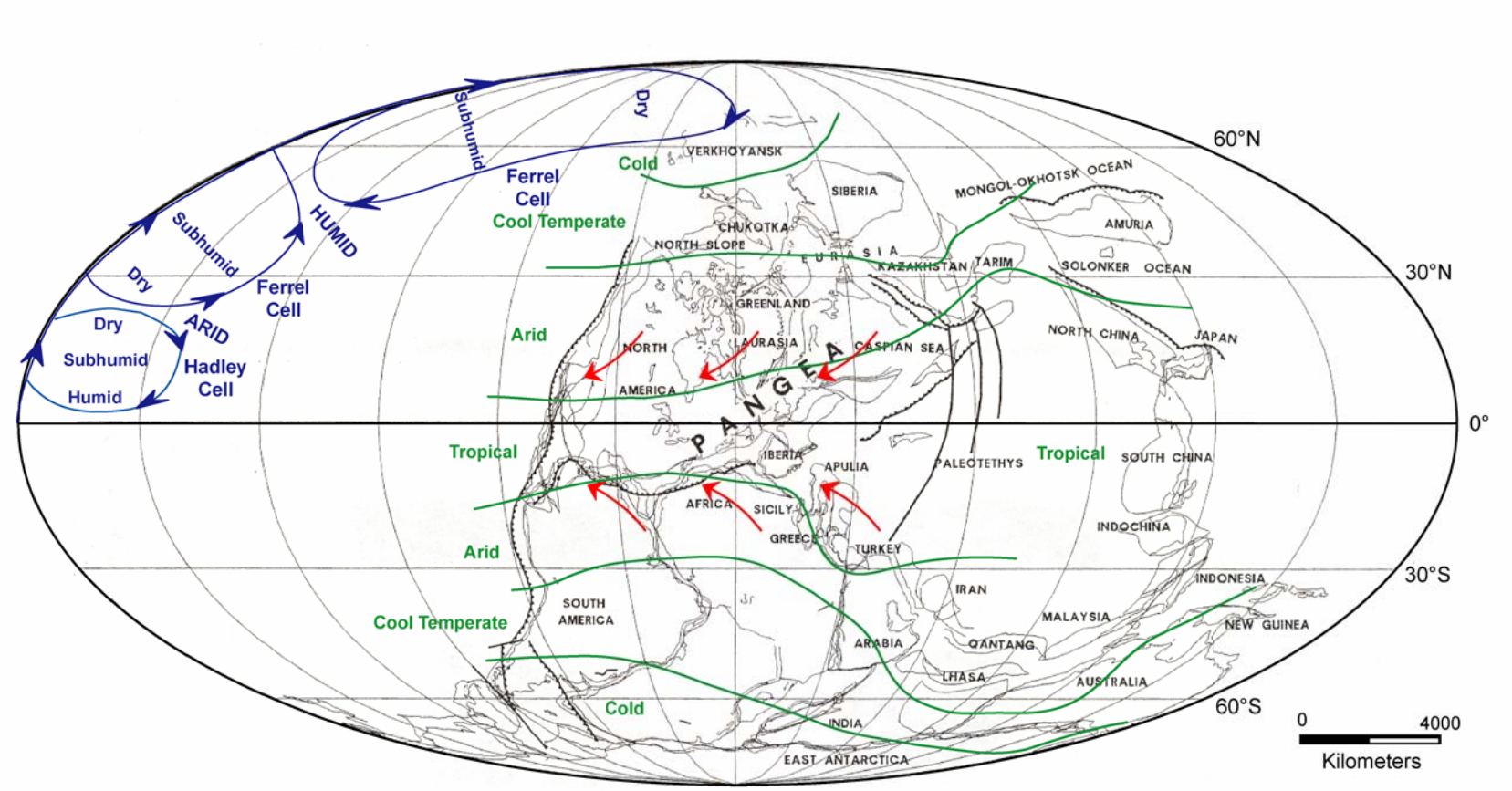

Figure 11. Paleogeographic map of the Lower Absaroka I time slice (adapted from Golonka, 2002). Superimposed on the tectonic map are climate interpretations in green (based on Scotese, 2000). The atmospheric cell circulation patterns in blue (based on Soreghan, 1994). Paleo-tradewind directions are marked in red.

APPENDIX A

DEFINITION OF TEXTURES

MUDSTONE

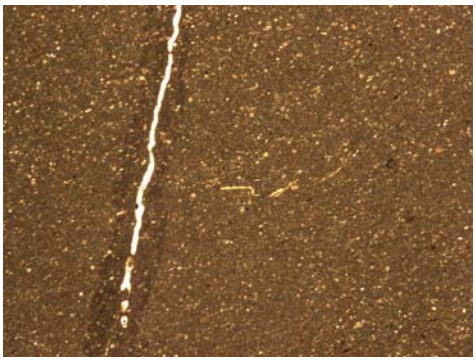

Sample M-39A (2x magnification).

- Massive to silty laminated mud
- 67-98% lime mud matrix
- < 10% grains
- Deposited along low-energy, distal outer ramp

MICROBIOCLASTIC MUDSTONE

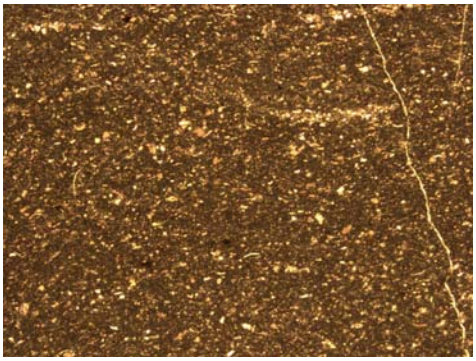

Sample M-26F (2x magnification).

- Muddy matrix (31-96%) with abundant microbioclasts, defined as finely commuted skeletal grains, see (Leavitt, 2002)
- < 10% grains
- Deposited along outer ramp or in restricted inner ramp, where energy levels are low with occasional gravity flows and storm suspensions

WACKESTONE

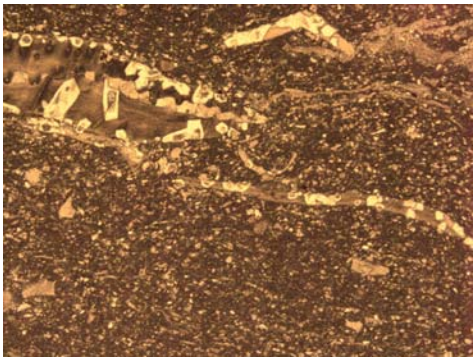

A wackestone with a microbioclastic matrix; sample M-44C (2x magnification).

- Mud-supported matrix
- 30-88% lime mud
- > 10% grains
- Deposited in low to moderate energy environments

MUD-DOMINATED PACKSTONE

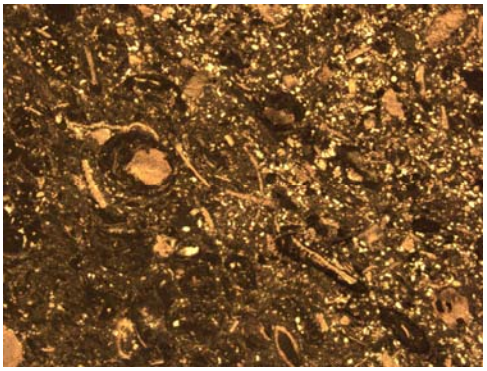

Sample M-42H (2x magnification).

- 16-70% lime mud
- Grain-supported
- Deposited along proximal outer ramp and inner ramp where energy levels are moderate to high

GRAIN-DOMINATED PACKSTONE

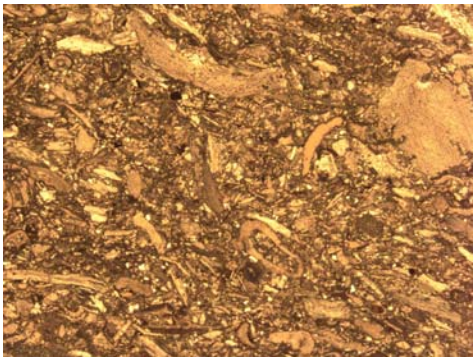

Sample M-12D (2x magnification).

- 4-57% lime mud
- Grain-supported
- Often over-packed due to chemical and mechanical compaction
- Deposited along moderate- to high-energy portions of inner and outer ramp

GRAINSTONE

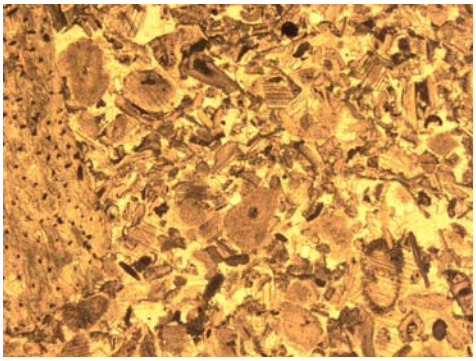

Sample M-2D (2x magnification).

- Grain-supported
- Sparry calcite cement and/or significantly low levels of mud to no mud at all
- Deposited in high-energy shoal and foreshore environments

DETAILED SEQUENCE STRATIGRAPHIC CHART for MORROWAN STRATA of the BIRD SPRING FORMATION, ARROW CANYON, CLARK COUNTY, NEVADA

FISCHER DIAGRAM

CYCLE NAME

LAI-B1.1 LAI-B2.1 LAI-B3.1 LAI-B4.1 LAI-B5.1 LAI-B6.1 LAI-B7.1 LAI-B8.1 LAI-B9.1 LAI-B10.1 LAI-B11.1 A-2 A-6 A-11 A-16 D-1 D-6 D-10 D-15 D-18 D-24 D-28/29'

SEQUENCE BOUNDARIES

CUMULATIVE DEVIATION FROM MEAN THICKNESS

-10 -20 -30 -40 -50 -60

SEQUENCE LAI-B11

SEQUENCE LAI-B10

SEQUENCE LAI-B9

SEQUENCE LAI-B8

SEQUENCE LAI-B7

SEQUENCE LAI-B6

SEQUENCE LAI-B5

SEQUENCE LAI-B4

SEQUENCE LAI-B3

SEQUENCE LAI-B2

SEQUENCE LAI-B1

250 200 150 100 50 0

Meters above base of section

Sea-level rise (m)

Blue curve = 2nd-order sea-level curve
Black = 5th-order fluctuations during 3rd-order sequences

3rd-order Systems Tracts

5th-order Fundamental Cycles

SL RC FWWB SWB SF

White = Inner ramp
Gray = Proximal outer ramp
Black = Distal outer ramp

Base of cycle above Mid-Carboniferous boundary

LAI-B11.2 LAI-B11.1 LAI-B10.6 LAI-B10.5 LAI-B10.4 LAI-B10.3 LAI-B10.2 LAI-B10.1 LAI-B9.4 LAI-B9.3 LAI-B9.2 LAI-B9.1 LAI-B8.5 LAI-B8.4 LAI-B8.3 LAI-B8.2 LAI-B8.1 LAI-B7.4 LAI-B7.3 LAI-B7.2 LAI-B7.1 LAI-B6.6 LAI-B6.5 LAI-B6.4 LAI-B6.3 LAI-B6.2 LAI-B6.1 LAI-B5.6 LAI-B5.5 LAI-B5.4 LAI-B5.3 LAI-B5.2 LAI-B5.1 LAI-B4.4 LAI-B4.3 LAI-B4.2 LAI-B4.1 LAI-B3.7 LAI-B3.6 LAI-B3.5 LAI-B3.4 LAI-B3.3 LAI-B3.2 LAI-B3.1 LAI-B2.6 LAI-B2.5 LAI-B2.4 LAI-B2.3 LAI-B2.2 LAI-B2.1 LAI-B1.7 LAI-B1.6 LAI-B1.5 LAI-B1.4 LAI-B1.3 LAI-B1.2 LAI-B1.1 LAI-S0.2 LAI-S0.1

MOLLUSC (count per 300)

ALGAE (count per 300)

PELOIDS (count per 300)

ONCOIDS (count per 300)

QUARTZ GRAINS (count per 300)

50 100 150 200 250 300

LEGEND

DISTAL OUTER-RAMP FACIES (HETEROZOAN)

- Facies 0: Laminated mudstone facies
- Facies 1: Burrowed mudstone to sparse wackestone facies
- Facies 2: Heterozoan skeletal wackestone facies

PROXIMAL OUTER-RAMP FACIES (HETEROZOAN TO TRANSITIONAL)

- Facies 3: Transgressive skeletal packstone facies
- Facies 4: Over-packed crinoid packstone facies
- Facies 5: Mixed heterozoan/photozoan wackestone to grain-dominated packstone facies

INNER-RAMP FACIES (PHOTOZOAN)

- Facies 6: Oncoidal packstone to grainstone facies
- Facies 7: High-energy shoal grainstone facies
- Facies 8: High-energy laminated foreshore facies
- Facies 9: Lagoonal packstone to grainstone facies
- Facies 10: Peritidal laminite facies
- Facies 11: Lowstand mixed siliciclastic-carbonate facies
- Soil horizon
- Sand overlay indicating abundant eolian quartz grains in sample

FUNDAMENTAL CYCLE TYPES

- Shallow photozoan cycle
- Mixed heterozoan/photozoan cycle
- Deep subtidal cycle

SEQUENCE STRATIGRAPHY & SYSTEMS TRACTS

- HST Highstand System Tract
- TST Transgressive System Tract
- LST Lowstand System Tract
- Sequence Boundary
- Transgressive Surface
- Maximun Flooding Surface
- Cycle Boundary

Figure 8. Detailed sequence stratigraphic chart for Morrowan strata of the Bird Spring Formation, Arrow Canyon, Clark County, Nevada. The top portion of this data chart contains a Fischer diagram for the Morrowan through Desmoinesian cycles located in Arrow Canyon. This illustrates that accommodation on an average remained unfilled throughout the Morrowan. At the far left of the chart are several graphs which plot petrographic thin section point-count data for molluscs, algae, peloids, quartz grains, and oncoids. Notice that the oncoids and quartz grains are rare or absent during second-order flooding conditions. Also, several of these photozoan compositional components become more abundant during third-order sequence boundaries. Moving to the right of the chart, notice the second-order sea-level curve, the third-order systems tracts, the fifth-order fundamental cycle stacking patterns, and the facies stacking patterns. The white, gray, and black blocks in the far right column signify where each portion of the cycle was deposited along the Bird Spring carbonate ramp: white, inner ramp; gray, proximal outer ramp; black, distal outer ramp. At the far right are the fifth-order fundamental cycle labels.

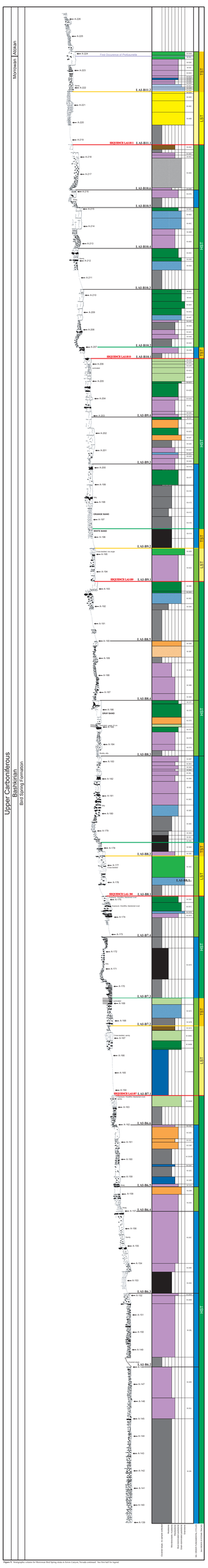

Figure 9. Stratigraphic column for Morrowan Bird Spring strata in Arrow Canyon, Nevada continued. See first half for legend.

Figure 9. Stratigraphic column for Morrowan Bird Spring strata in Arrow Canyon, Nevada. To the far left notice the Amoco measured section. Each number preceded by the letter A (i.e., A-56) corresponds with Amoco outcrop reference markers placed at 1.5-m intervals. The column is subdivided into 59 fifth-order fundamental cycles, which are labeled according to their stratigraphic placement within third-order sequences (i.e., LAI-B1.1 = Lower Absaroka Ia supersequence, Bashkirian stage, Sequence 1, Cycle 1). The colored column directly to the right of the Amoco measured section is the log of facies (profile of log = texture classification; color of log = facies classification). To the right of the facies log is a column indicating the spacing of petrographic samples. The next column shows fundamental cycle classification (see legend for color coding). Finally, the far left column indicates the third-order systems tract subdivisions. Sequence boundaries, transgressive surfaces, and maximum flooding surfaces are also noted (see legend). Third-order sequence bases are labeled according to their stratigraphic placement in the Lower Absaroka Ia supersequence (i.e., Sequence LA-B1 = Lower Absaroka Ia supersequence, Bashkirian stage, third-order sequence 1). Note that S = Serpukhovian.